

NASA Technical Memorandum 88211

**Final Report on the Static
Calibration of the RSRA
Active-Isolator Rotor
Balance System**

C. W. Acree, Jr.

MARCH 1987

NASA

NASA Technical Memorandum 88211

**Final Report on the Static
Calibration of the RSRA
Active-Isolator Rotor
Balance System**

C. W. Acree, Jr.
*Ames Research Center
Moffett Field, California*



National Aeronautics
and Space Administration

Scientific and Technical
Information Branch

1987

NOMENCLATURE

a, b, c, d, e, f, g, h	isolator system dimensions, defined in figure B1
a_i	coefficients of separation-line polynomial
b_s	intercept of separation-line polynomial
C_1, C_2, C_3	dimensional constants, defined in appendix B
d_l, d_u	lower- and upper-band adjustments for hysteresis
e_l, e_u	errors of the lower and upper separation lines
F_t	torque linkage tension
I_1, I_2, I_3	isolator outputs (fig. B1)
k_1, k_2, k_3	torque linkage dimensions, defined in figure B2
L_1, L_2, L_3, L_4	load cell outputs (fig. B2)
m_s	slope of the separation line
n_l, n_u	number of data points in each hysteresis band
n_s	order of the separation-line polynomial
T_1, T_2	torque couple applied to torque linkage
X, Y, Z, L, M, N	forces and moments at the rotor head (shown in fig. 1 and defined in table 1)
X', Y', Z', L', M', N'	forces and moments in an axis system aligned with the torque linkage (fig. B1)
x_l, x_u	applied loads, separated into hysteresis bands
x_s	original (unseparated) applied loads
y_l, y_u	errors, separated into hysteresis bands
y_s	unseparated errors (estimated)
α	load cell cant angle
Θ	torque linkage alignment angle (fig. B2)
σ	standard deviation
Matrix and Vector Quantities	
B	regression intercepts = calibration offsets
C	regression coefficients = calibration matrices

F	true rotor loads
\hat{F}	estimated rotor loads
L	transducer outputs (load cells, isolators, etc.)

Subscripts and Superscripts

i	order of individual polynomial term
ℓ	lower hysteresis band
u	upper hysteresis band
s	separation line

SUMMARY

The Rotor Systems Research Aircraft (RSRA) active-isolator system is designed to reduce rotor vibrations transmitted to the airframe and to simultaneously measure all six forces and moments generated by the rotor. These loads are measured by using a combination of load cells, strain gages, and hydropneumatic active isolators with built-in pressure gages. The first static calibration of the complete active-isolator rotor balance system was performed in 1983 to verify its load-measurement capabilities. Analysis of the data included the use of multiple linear regressions to determine calibration matrices for different data sets and a hysteresis-removal algorithm to estimate in-flight measurement errors. Results showed that the active-isolator system can fulfill most performance predictions. The results also suggested several possible improvements to the system.

INTRODUCTION

The Rotor Systems Research Aircraft (RSRA) has stringent requirements for vibration reduction and rotor loads measurement. The active-isolator rotor balance system is designed to meet both requirements simultaneously. Flight tests had demonstrated the system's basic operational feasibility; however, the load-measurement capability, which is necessary for rotor performance research, remained unverified until the full system was calibrated in early 1983.

There are two versions of the RSRA. One is configured as a compound helicopter, as shown in figure 1; the other is a pure helicopter, as shown in figure 2. (The pure helicopter is without the wing, auxiliary thrust engines, or lower horizontal stabilizer of the compound helicopter.) A more complete general description of the RSRA is given by Burks (ref. 1).

This paper presents the calibration of the active-isolator system which was installed in the pure helicopter version of the RSRA. (This aircraft is now being converted into the X-Wing research aircraft.) The axis system shown in figure 1 was used for all calibration loads throughout this paper.

An earlier paper by this author (ref. 2) describes the calibration results of the compound version of the RSRA. (That aircraft can be fitted with the active-isolator system as required for research.) It also has an entirely different rotor-load measurement system with no vibration reduction capability; consequently, the calibrations and analytical results are completely independent. The distinctions between the two aircraft and the two load-measurement systems should be kept in mind when interpreting the information presented in this report.

This paper consolidates material from several previous papers into a self-contained final report and presents the results of an improved hysteresis-removal algorithm. Reference 3 contains extensive plots of the raw data. Reference 4 presents additional plots and an appendix which discusses

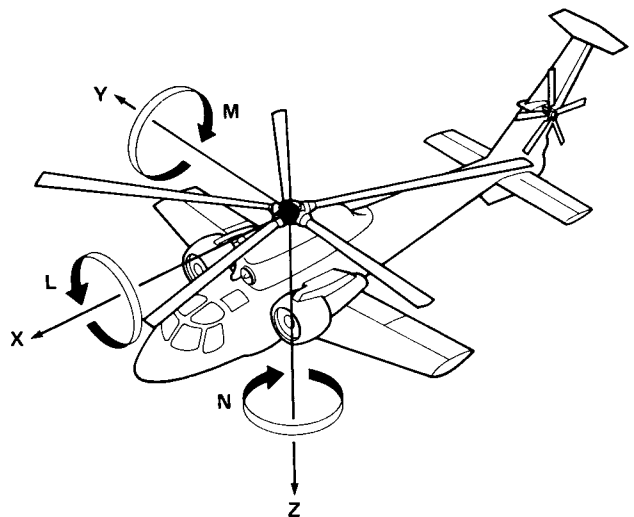


Figure 1.— RSRA compound version with load-measurement axis system.

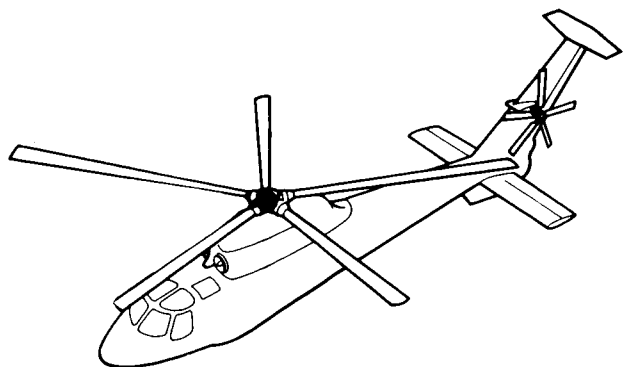


Figure 2.— RSRA pure helicopter version.

the initial results of the regression technique used for calibration analysis. Reference 5 extends the analysis to include a hysteresis-removal algorithm. The concept and design of the active-isolator system are discussed in references 6 and 7.

Analytical procedures were based on those described in reference 2. For the active-isolator calibration, the calibration loads were thoroughly revised and a direct multiple linear regression was used almost exclusively. For the present report, an advanced hysteresis-removal algorithm was developed to better predict the expected in-flight performance of the system.

Topics covered in this report include (1) a description of the RSRA active-isolator rotor balance system; (2) requirements imposed by rotor research programs; (3) techniques for the static load calibration; (4) data analysis, including linear regression and methods of hysteresis removal; and (5) improvements and options for support of future research. Three appendices are also included: Appendix A is a tabulation of key calibration matrices, B is a derivation of an ideal ("geometric") calibration matrix, and C shows plots of corrected responses to calibration load inputs for three reference data sets.

THE ACTIVE-ISOLATOR SYSTEM

The rationale for the design of the original active-isolator system is discussed by Walton, Hedgepeth, and Bartlett (ref. 6). The design details described by Kuczynski and Madden (ref. 7) are summarized here. Key functions are the reduction of vibratory rotor loads transmitted to the fuselage and the measurement of net steady forces and moments. Full-system calibration is necessary to verify proper operation and to ensure that all measurements are traceable to the National Bureau of Standards.

System Description

Figure 3 shows the basic concept of RSRA rotor-load measurement, whereby rotor loads are transmitted from the base of the transmission to the airframe through a collection of force transducers. The layout of the active-isolator rotor-load measurement system is shown in more detail in figure 4 (see also appendix B). The main rotor transmission is mounted to a baseplate, which is in turn connected to the airframe by the load-measurement system. Four vertical load cells in a focused configuration take up vertical loads, and four hydropneumatic isolators react in-plane loads. The load cells are canted 15° inward at the bottom toward the extended main rotor shaft centerline. In addition, a torque linkage (partly hidden in the figure) allows free translation in the horizontal plane, but resists in-plane rotation. The aft

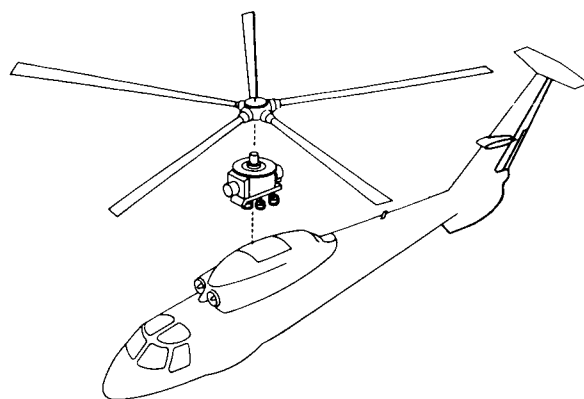


Figure 3.— RSRA pure helicopter version, showing the concept of rotor-load measurement.

isolator is a safety backup unit, and is not normally activated or loaded in flight.

The entire system functions analogously to a wind-tunnel balance for rotor-load measurement. Vibrations in the horizontal plane are isolated from the airframe, but vertical loads are not isolated. Adding the active isolators to the RSRA would allow testing rotors whose vibratory characteristics would otherwise preclude flying them on the basic airframe, while retaining full use of the RSRA's unique data-collection capability for rotor performance measurements.

Figure 5 schematically illustrates an active-isolator unit. Loads are carried by a piston moving in a cylinder filled with hydraulic fluid. Each end of the cylinder is connected to an accumulator, where a flexible diaphragm separates the fluid from an air chamber. The air chambers act as pneumatic springs to absorb vibratory loads, and a servo valve keeps the piston centered under large steady loads. Hydraulic power is supplied by conventional aircraft hydraulic pumps. A differential pressure transducer provides load data. In the event of isolator or hydraulic system failure, a piston lock creates a separate load path for safety. The servo-valve feedback gains and the accumulator precharge pressures may be altered as needed to match different rotors or different testing requirements.

The torque linkage provides structural redundancy for safety: it reacts the large, steady torque loads if an isolator unit should fail. Three load tubes and two bellcranks compose the torque linkage; the airframe itself and the transmission baseplate make up the last two elements of a seven-bar linkage with two degrees of freedom. The transmission is restrained from rotation, but is otherwise free to translate in the horizontal plane, allowing in-plane loads to be taken up by the load cells and isolators. The linkage is pre-loaded so that, at normal rotor torques, the two lateral isolators are loaded near the middle of their operating range and share the torque loads with the linkage. One of the linkage tubes has

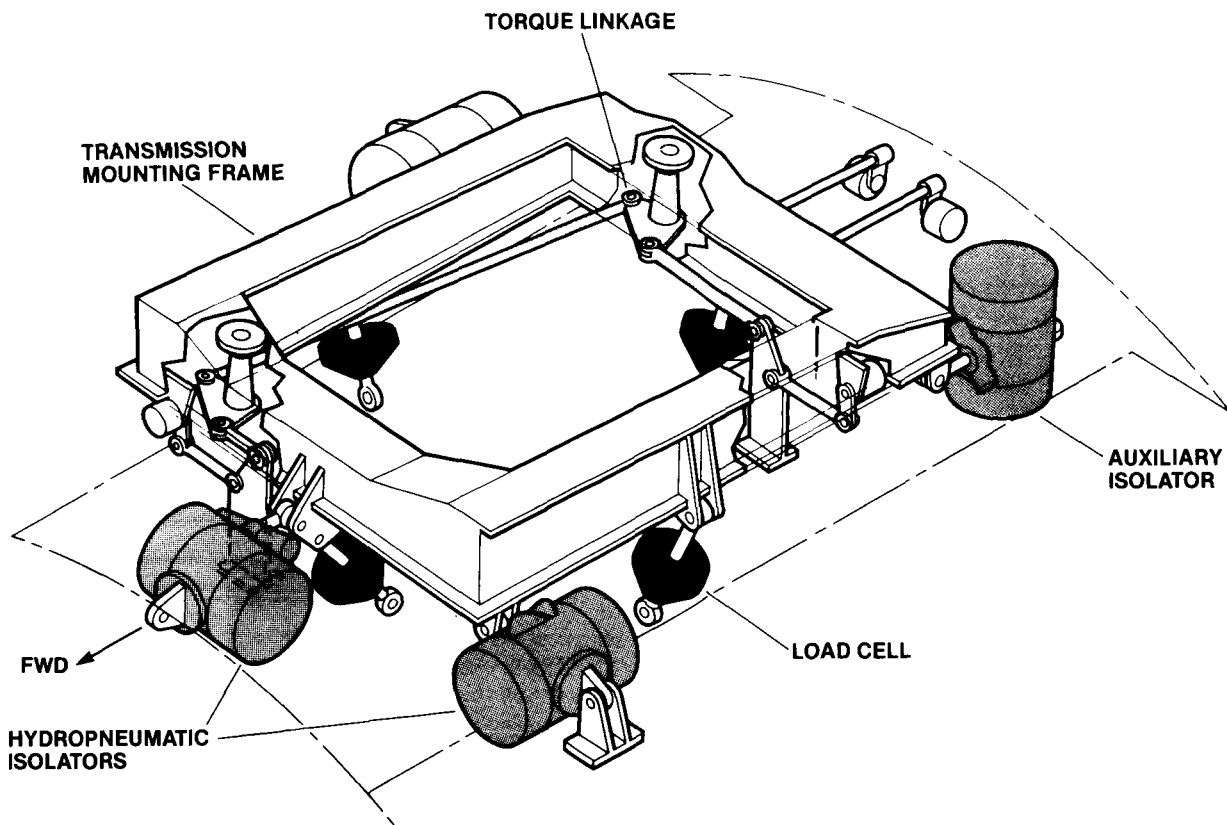


Figure 4.— RSRA active-isolator rotor-load measurement system.

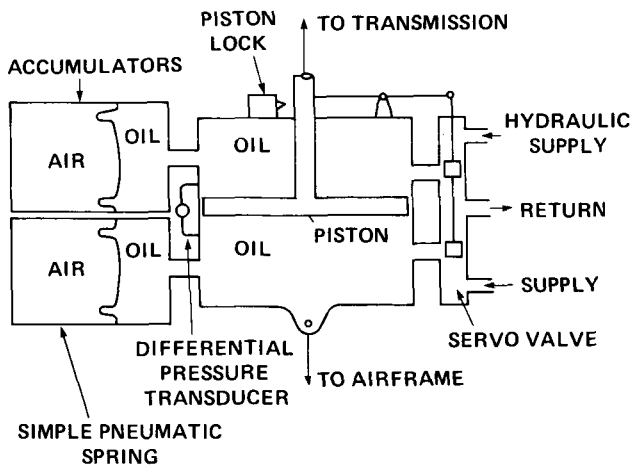


Figure 5.— Schematic of RSRA active-isolator unit.

conventional strain gages which permit torque-linkage loads to be monitored and used as calibration data.

In order to isolate rotor vibrations from the airframe, the active isolators must allow the transmission to move slightly with respect to the rest of the aircraft. This motion (up to ± 0.21 in.) would apply undesired control inputs to the rotor through motion relative to the flight controls, which are

normally grounded to the airframe. A special mechanical motion-compensation system (ref. 8) eliminates this effect by adding corrective motions to the flight control linkages. The system is designed so that applied, corrective, and reaction control forces all cancel at the transmission, preventing any net unmeasured control forces from being applied to the rotor or transmission. There are some residual linkage moments, but these are negligible compared to aerodynamic rotor loads. There is also some linkage bearing friction, which is also negligible.

Research Requirements

Even though there are many different devices for eliminating rotor vibration, only the RSRA active-isolator system can be readily tailored to a wide variety of rotors without a complete system remanufacture or redesign. Moreover, the system also provides simultaneous measurements of all rotor forces and moments in flight, which is an essential requirement for the RSRA.

Design of the active-isolator system was directed solely toward meeting research requirements, such as measurement of flight loads and adjustability to accommodate different rotors. It was not intended that the system be readily adaptable to production aircraft.

The concept of "active isolation" has been refined continuously since the RSRA active isolators were designed. Several methods of using airframe vibration measurements as feedback signals to isolation devices or to the control system have been proposed and tested; a familiar example is higher-harmonic control. The RSRA isolators have no such global feedback capability; their servo valves are for self-centering only.

Three major requirements were established for the active-isolator system (ref. 6): (1) reduction of rotor vibrations transmitted to the airframe; (2) measurement of static rotor loads; and (3) measurement of dynamic rotor loads. Flight tests and a limited shake test (ref. 7) verified that the system could meet the first requirement. As shown below, the static calibration demonstrated that the second requirement can also be met. The dynamic-load measurement capabilities remain unverified. However, note that vibration reduction and static-load measurement had to be demonstrated before dynamic calibration could be realistically specified. The present level of system development allows calibrated rotor performance measurements to be made in flight, even without a dynamic calibration.

Figures 6 and 7 show vertical accelerations at the pilots' station in response to main-rotor longitudinal and lateral excitation, based on airframe shake test data (ref. 7). If a four-bladed rotor were to be flown on the RSRA, the four-per-revolution frequency would fall almost exactly at the airframe peak response. As shown in the figures, use of the active isolators reduces the vibratory response and would allow a representative modern rotor to be tested at current RSRA transmission speeds.

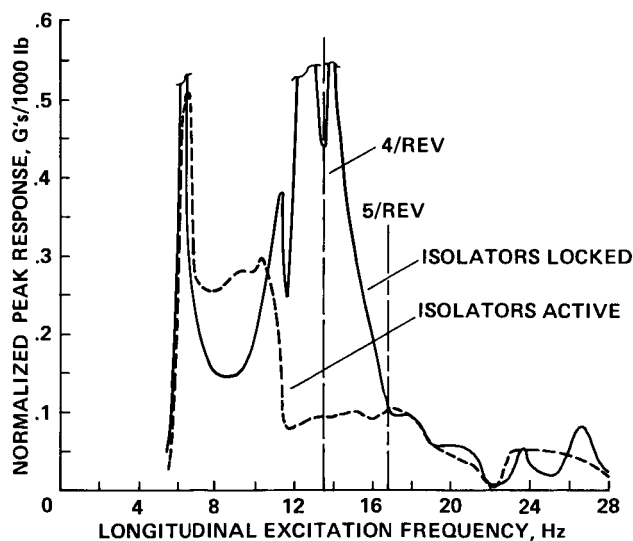


Figure 6.— Effect of the isolation system on pilot vertical response to rotor longitudinal excitation (shake test results from ref. 7).

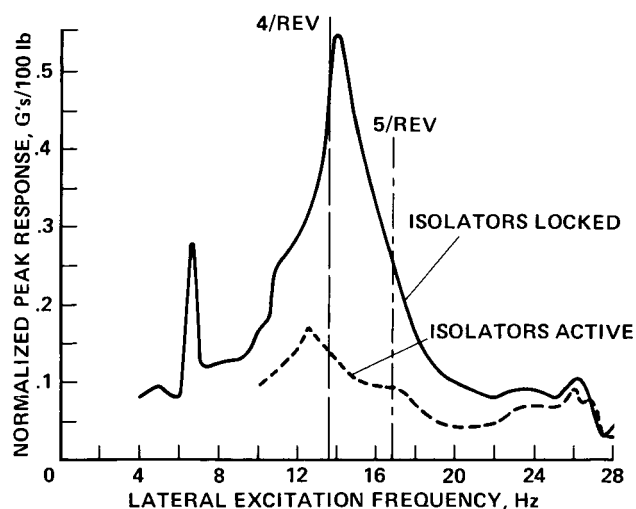


Figure 7.— Effect of the isolation system on pilot vertical response to rotor lateral excitation (shake test results from ref. 7).

Calibration Requirements and Techniques

It is required that rotor forces and moments be measured with accuracies traceable to the National Bureau of Standards. However, calibrations of individual components are not sufficient for those purposes. Structural flexibility in the airframe changes the load distribution among the active isolators, load cells, and torque linkage, which causes interactions (cross-coupling) and changes in effective sensitivities. As will be shown later in this paper, these nonrandom errors are significant. Furthermore, the isolator pistons must move slightly to absorb vibration, and any motion under static loads will further change the load distribution. Isolator internal friction and accumulated rigging (alignment) errors accentuate the problem. Consequently, the entire load-measurement system must be calibrated after it is installed in the aircraft. Proper analysis of a full-system calibration can eliminate nonrandom linear errors (systematic errors), and can reduce the effects of other errors by adjusting the calibration coefficients in the data reduction equations.

Figure 8 illustrates the static calibration method, which was essentially the same as that used on the compound version of the RSRA (ref. 3). A special calibration fixture replaced the rotor head, and the airframe was restrained by the landing gear mounting lugs. Through cables and pulleys, hydraulic cylinders applied static loads. For lift, however, a solid rod and walking beam were used. High-accuracy load cells, suitable for calibration reference, connected the cables and rod directly to the rotor-head fixture. The fixture was designed for very high stiffness and was fitted with inclinometers. This ensured that all calibration loads could be resolved at the center of the rotor shaft, in the plane of the flapping

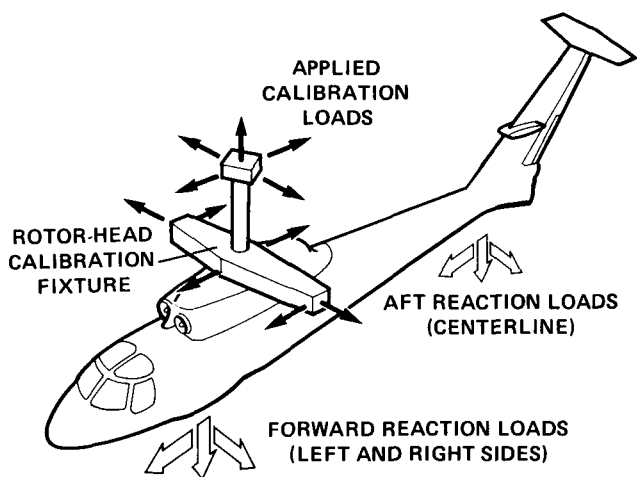


Figure 8.— Method of applying calibration loads to the RSRA.

meter connected to a high-speed scanner, and various accessories (such as a small printer) were connected to a parallel data bus. The aircraft load cells and isolator pressure transducers, and the calibration-reference load cells, were sequentially sampled to take calibration data. The voltmeter errors were much smaller than any other errors. Also, the scanning rate was fast enough so that load drift during each data scan was less than its respective reference calibration accuracy (table 1). This allowed the calibration data to be treated as if each scan were perfectly simultaneous and error free. The computer converted raw voltage readings to engineering units, displayed selected parameters in real time, and stored all data on command. A small local disk drive provided temporary data storage; all data were eventually transferred to a large mainframe computer for editing, plotting, and analyzing.

PREDICTIONS AND TEST RESULTS

Predicted Measurement Errors

A simple check of system performance consists of comparing predicted loads to known applied loads. This requires a calibration matrix which transforms raw transducer outputs to resultant loads in the same coordinate system that is used for calibration (fig. 1). For this performance check, a simple matrix based on design geometry was used. It was derived by requiring that the sum of the loads in the torque linkage and all load cells and isolators must equal the loads applied at the rotor head. One must also correct for the angles and the distances between the transducer measurement axes and the rotor head coordinate axes in which calibration loads were applied. The values of the matrix elements are given in appendix A; their derivations are summarized in appendix B.

If the active isolators performed perfectly and if the airframe were completely rigid, measurement accuracy would be limited only by pressure-transducer and load-cell accuracies. Equivalent measurement root-mean-square (rms) errors

hinges, regardless of applied load level and any airframe deflections.

The reference axis system shown in figure 1 is used for all calibration loads in this paper. Table 1 lists the values of the applied loads. The single loads represent the performance limits of the S-61 rotor currently installed on the RSRA. The combination loads are reduced because of structural limitations of the airframe when it is installed in the calibration facility. The most important combined loads are those with lift (Z) and torque (N), because these two loads are significant for virtually all reasonable flight conditions.

The calibration-reference load cells were individually calibrated with equipment whose accuracies were traceable to the National Bureau of Standards. Such calibrations of the reference load cells determined the facility accuracies given in table 1. The listed values are the standard deviations of the errors in measuring each applied load (rounded upward to be conservative).

Figure 9 is a simple schematic of the calibration data system (ref. 9). A desktop computer controlled a digital volt-

TABLE 1.— CALIBRATION-FACILITY STATIC LOAD APPLICATION CAPABILITIES (1983-1984)

Applied-load axis	Positive direction	Single load limit (100%)	Combination load limit	Applied-load accuracy
X (longitudinal)	Forward	±8,620 lb	±4,000 lb	13 lb, 0.2% ^a
Y (lateral)	Right	±5,420 lb	±2,500 lb	11 lb, 0.2%
Z (vertical)	Down	-48,800 lb	-24,400 lb	47 lb, 0.1%
L (roll)	Right down	±16,667 ft-lb	±8,333 ft-lb	42 ft-lb, 0.3%
M (pitch)	Nose up	+25,000 ft-lb (-16,667 ft-lb)	±12,500 ft-lb	50 ft-lb, 0.2%
N (torque)	Left forward	+58,167 ft-lb	+50,000 ft-lb	25 ft-lb, 0.05%

^aPercent full scale.

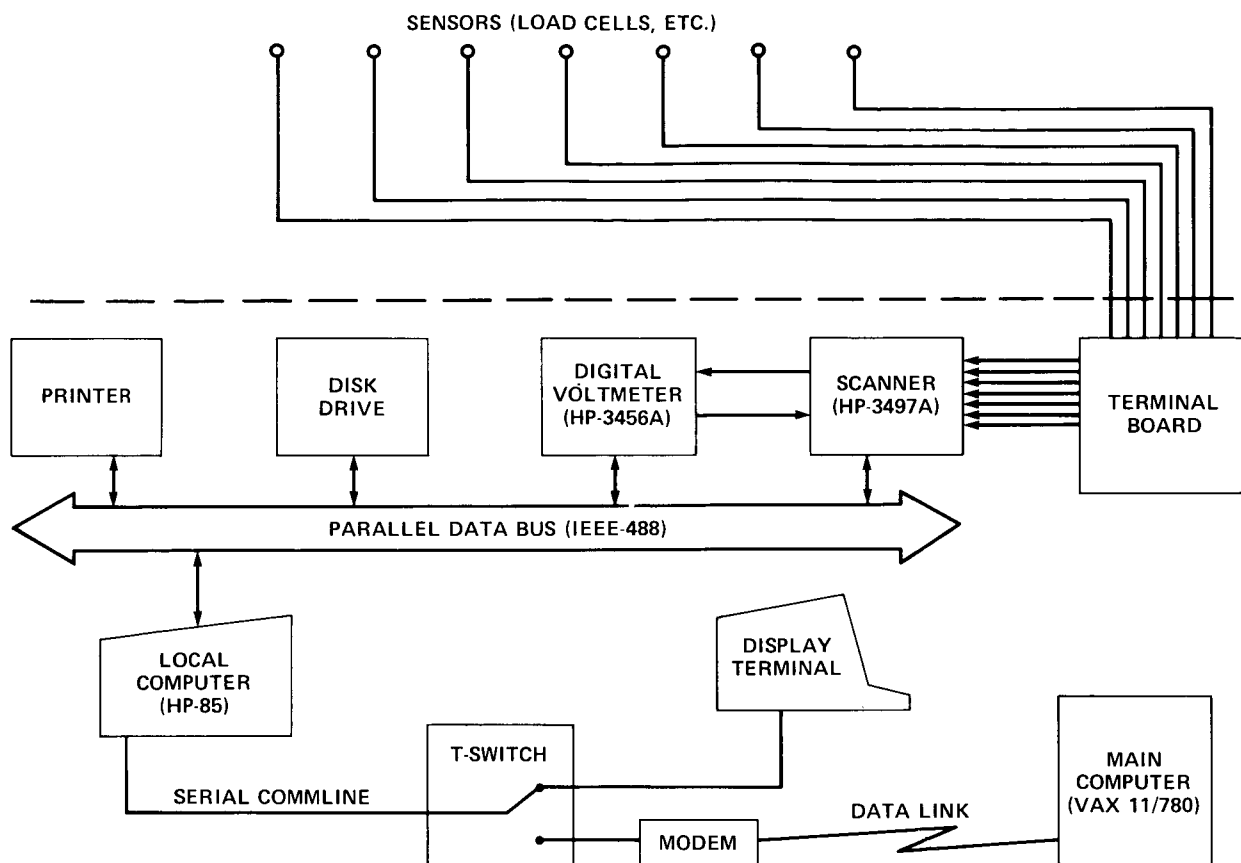


Figure 9.— Simplified schematic of the calibration data system.

based on this assumption are given in table 2 in the column labeled "transducer errors." The values are derived from individual component calibrations performed shortly before the full-system calibration, with the results converted to equivalent rotor loads by propagating the errors through the

geometric matrix. They do not include torque linkage or aft isolator errors because the torque linkage was not highly loaded at maximum applied torque load, and the aft isolator was not activated during the system calibration.

TABLE 2.— PREDICTED MEASUREMENT ERRORS

Applied-load axis	Full-scale load limit	Transducer errors ^a	Full-system errors ^b	Geometric-matrix errors ^c
X, lb	±8,620	74	177	314
Y, lb	±5,420	121	171	232
Z, lb	-48,800	31	47	110
L, ft-lb	±16,667	578	893	992
M, ft-lb	+25,000	328	687	1064
N, ft-lb	-16,667			
	+58,167	180	302	3489

^aExcluding torque linkage or aft isolator errors.

^bRepresentative of 120-knot level flight.

^cRms errors, averaged over all full-scale loads.

For comparison, table 2 also presents predictions¹ of total system errors, including all expected sources of error based on limited laboratory tests. These errors include individual load-cell force-measurement errors, isolator pressure-transducer measurement errors, and breakout friction in the assembled system. Of the several sources of friction, the most important are (1) isolator and load-cell rod-end bearings, (2) torque-linkage bellcrank and rod-end bearings, and (3) isolator piston sliding seals. Friction levels were based on system design loads characteristic of 120-knot level flight. The sums of all of these errors are listed in table 2 under "full-system errors."

Predicted Versus Applied Loads

The results of converting calibration data by using the geometric matrix are plotted as predicted loads against known applied loads in figures 10-15. Only single loads (case 1 in table 3, discussed in the next section) are plotted. For these plots, all loads were normalized with respect to the maximum loads in each axis (table 1). All six predicted loads could therefore be shown on the same plot for each applied load, allowing direct comparison of relative accuracies. A perfect prediction in the same axis as the applied load would be a diagonal line with a slope of unity (the dashed reference line in each plot). Perfect predictions in all other axes would be exactly zero.

(Similar plots are given in appendix C for the single-loads data set and two other data sets, but with calibration matrices derived by regression analyses. The regressions are discussed in the next section.)

The main rotor shaft of the RSRA is inclined 2° forward with respect to the airframe. Calibration was simplified by attaching the aircraft to the calibration facility framework in a 2° nose-up attitude, thereby orienting the main rotor shaft exactly vertically. This ensured that the weight of the transmission plus the rotor-head calibration fixture caused only constant, known biases in the calibration loads.

In normal flight conditions, there is a large, constant torque load. To compensate for this torque, the two lateral isolators are hydraulically preloaded so that they will operate near the middle of their measurement range. This introduces a preload into the torque linkage, also. These preloads introduced more biases during calibration.

A full calibration analysis (described later) would determine the best possible corrections for all biases, but the geometric matrix does not make such corrections. To simplify the data plots given in figures 10-15, the data were empirically adjusted by subtracting the biases, which were simply the mean errors in each axis before adjustment. This resulted in zero overall mean errors for all single loads. The plots thus reveal slope errors, asymmetry, nonrepeatability,

hysteresis, and other nonlinearities. Note that any given plot may show a bias in a particular axis; only the total biases (averaged over all loads) were removed.

Rms errors in predicting loads with the geometric matrix are given in table 2. Before calculating the rms values (which was done for all applied loads), biases were removed. The results thus closely approximate, but are not exactly identical to, true standard deviations. The statistics correspond exactly to the data as shown in figures 10-15, which do not show biases.

The most obvious problem is the severe slope error in torque (*N*) loads. Appendix A lists the geometric matrix and the single-loads matrix; comparing the elements for torque response shows that the cause of the error lies in the prediction of torque-linkage sensitivity. (The regression analysis used to generate the single-loads matrix is described in the following section.) In contrast, the response coefficients of the two lateral isolators were predicted almost exactly. This is significant because these two isolators carry almost all torque loads not picked up by the torque linkage. In any event, torque errors alone are sufficiently great to prove the need for a full regression analysis.

Because of the large torque errors reported in references 3 and 4, the torque linkage was re-analyzed in greater detail (see appendix B). This led to a modified geometric matrix. The resulting errors in torque and roll are noticeably different, but not actually improved. Table 2 and figure 15 reflect these changes (as does figure 13, but only slightly). However, no changes in the conclusions of this or earlier reports are warranted.

Revision of the data sets to eliminate questionable data (caused by calibration equipment malfunctions) led to further, minor differences in the numerical results compared to those given in reference 3. A further consequence is that the plot of single *M*-load responses (fig. 14) is slightly different from the equivalent plot in reference 3. The changes were included in reference 4, and are not of major significance.

REGRESSION ANALYSIS

The Analytical Process

The calibration-correction equation may be written

$$\{F\} = [C]\{L\} + \{B\} \quad (1)$$

In flight, $\{F\}$ is the vector of six rotor loads (defined in fig. 1), which is to be determined. For calibration, $\{F\}$ is the vector of six applied calibration loads (dependent variables), taken one axis at a time, and $\{L\}$ is the vector of transducer outputs (independent variables). As many as 13 elements may be in $\{L\}$, although 8 are usually sufficient, as explained in the following section, Preliminary Analyses. The elements

¹Madden, J., RSRA AIB's Development Requirements. Unpublished memo, June 1979.

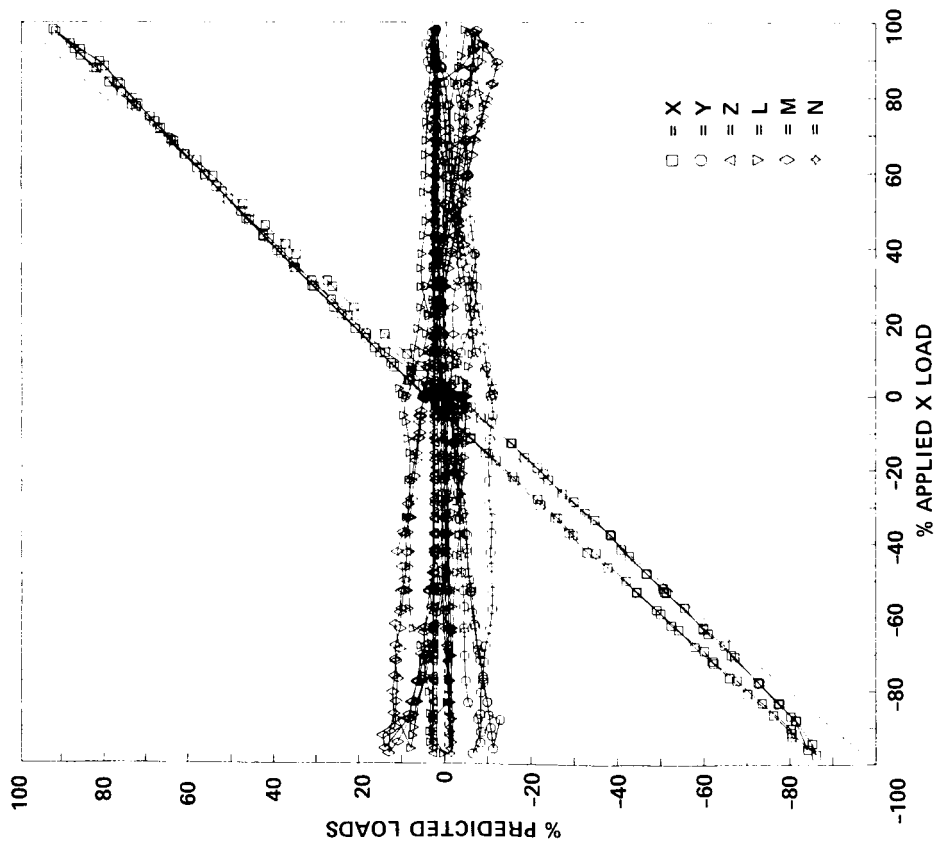


Figure 10.— Predicted loads for applied single X load, using the geometric matrix.

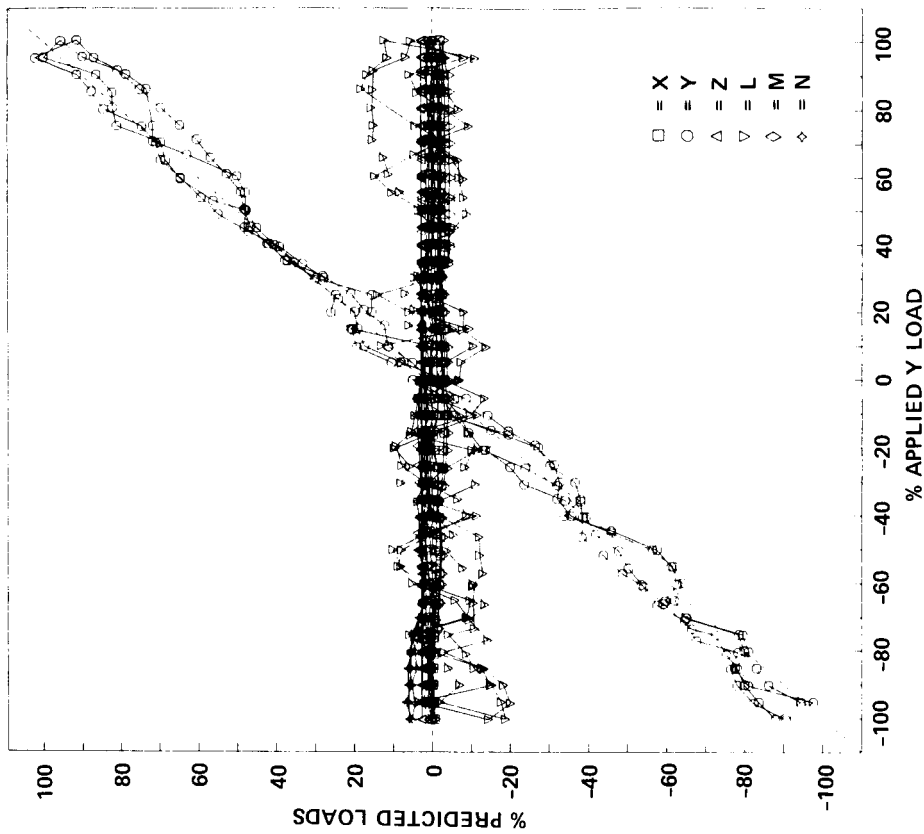


Figure 11.— Predicted loads for applied single Y load, using the geometric matrix.

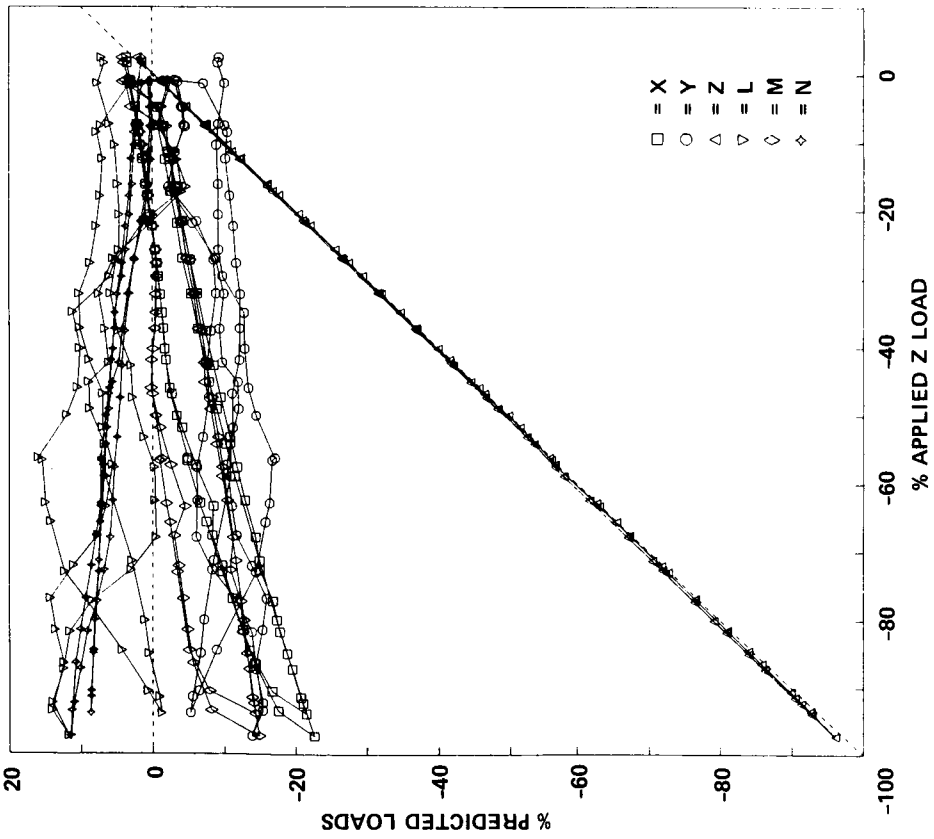


Figure 12.— Predicted loads for applied single Z load, using the geometric matrix.

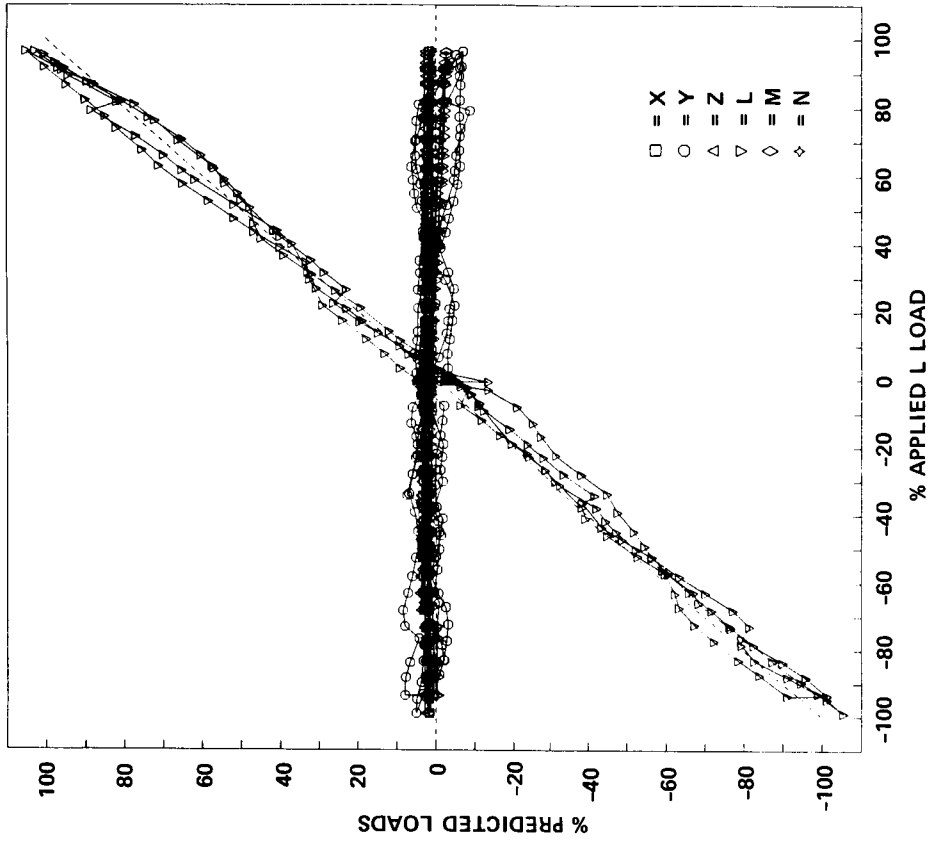


Figure 13.— Predicted loads for applied single L load, using the geometric matrix.

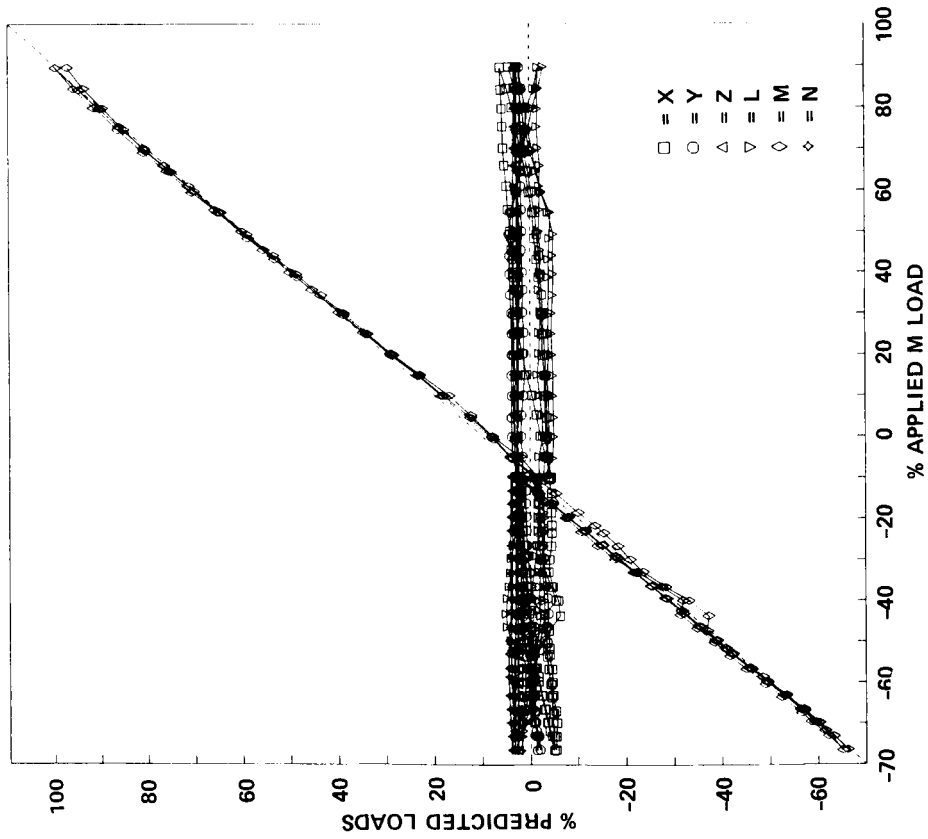


Figure 14.— Predicted loads for applied single M load, using the geometric matrix.

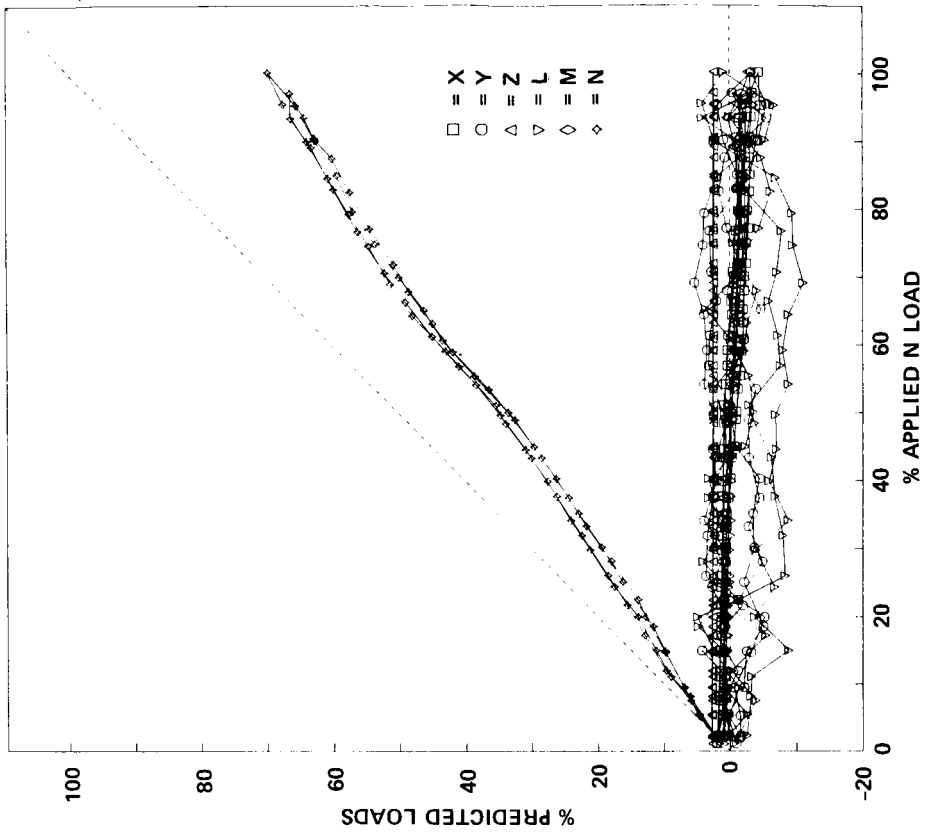


Figure 15.— Predicted loads for applied single N load, using the geometric matrix.

of each row of the calibration matrix $[C]$ are the regression coefficients for the corresponding axis of $\{F\}$. Each element of the intercept vector $\{B\}$ is derived simultaneously with a row of $[C]$. Once $[C]$ and $\{B\}$ have been determined from calibration data, they may be used to estimate loads in flight $\{\hat{F}\}$, so labeled because the exact true rotor loads $\{F\}$ are then unknown. $\{L\}$ is known exactly during both calibration and flight.

A regression gives statistically optimum results by adjusting correction coefficients (the calibration matrix elements) to compensate for such effects as manufacturing errors and airframe flexibility, which are not included in the geometric matrix. In addition, a stepwise regression also makes adjustments for differences among transducer accuracies.

A forward-stepwise multiple linear regression (ref. 10) was used to derive the calibration matrix and intercepts. Such a regression progressively adds statistically significant independent variables, one at a time. It should be noted that although the applied load vector $\{F\}$ is under the experimenter's control during the physical calibration, it must be treated as a vector of dependent variables by the regression. This is because the results of the regression, $[C]$ and $\{B\}$, are used to predict applied loads $\{\hat{F}\}$ from transducer data $\{L\}$.

For reduction of flight data, terms must be added to account for inertial effects that result from accelerations of the aircraft, including gravity. Derivation of inertial-effects corrections is not covered by this report; see reference 2 for the relevant equations. Also required for flight-data reduction is a vector of load tares to account for the difference in masses between the calibration fixtures attached to the aircraft and actual flight hardware. Calculation of the tare vector was not necessary for the analysis covered here.

Figure 16 is a flowchart of the analytical process. Note that calibration errors are not simply the regression standard errors. Those errors are conventionally defined as the errors in estimating the dependent variable, based on a single, entire data set. The procedures used here were generalized so that different calibration matrices could be tested to check for sub-optimal performance on the same reference data set. Also, errors in a given axis could be determined for applied loads in different axes. In particular, the error of most interest for a given axis is the root-mean-square (rms) error resulting from loads applied in the same axis. Such errors are generated by comparing predicted loads in a given axis (\hat{F} in fig. 16) with known calibration loads (F in the figure). The resulting initial error estimates are exact calibration errors (traceable to the National Bureau of Standards). In contrast, the errors generated by the hysteresis-removal algorithm (discussed below) are predictions of in-flight errors, and are so noted when presented. As indicated in figure 16, the known calibration loads are always used as the reference against which all errors are computed.

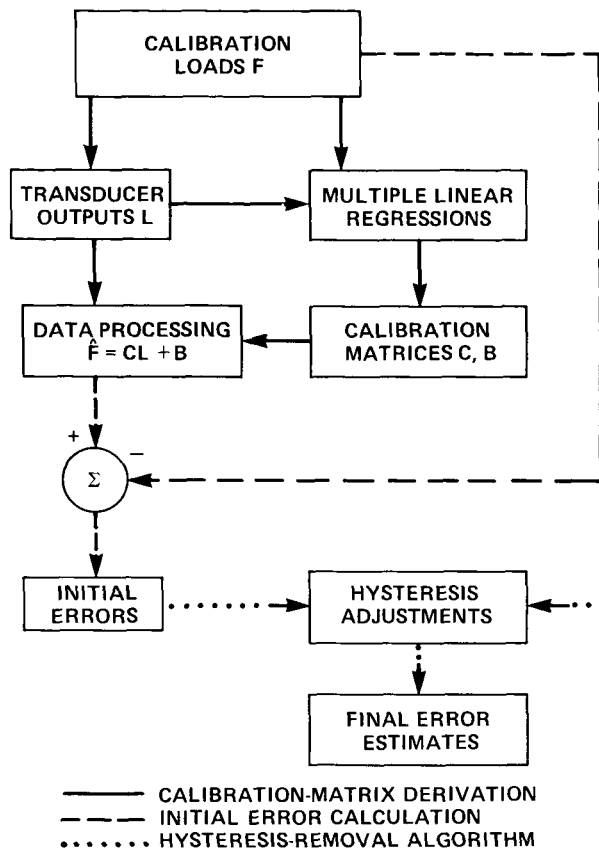


Figure 16.— Regression and error analysis flowchart.

Preliminary Analyses

Before discussing the results of the numerical analyses, a few general characteristics of the raw data should be mentioned. The zero-crossing errors and the data skew seen during the first RSRA calibration (ref. 2) were almost entirely absent from the isolator system calibration data (plotted in refs. 3 and 4). As the isolator system of the RSRA helicopter is inherently more susceptible to hysteresis errors than the all-load-cell system of the RSRA compound, the reduction of error almost certainly results from improved calibration procedures and equipment. Conventional, pure hysteresis errors are still present.

Inverse-regression analysis, used with success in the calibration of the RSRA compound (ref. 2), could not be used here. For an inverse regression, the roles of dependent and independent variables $\{F\}$ and $\{L\}$ are reversed. The resulting inverse calibration matrix must be converted into a proper calibration matrix $[C]$ by a pseudo-inverse matrix operation.

The problem with such an analysis is caused by nonlinear torque-linkage response, shown for single torque (N) loads in

figure 17. In order to accommodate the large, steady torque loads experienced in flight, both lateral isolators have opposing preloads to react the torque. The torque linkage also has a large preload, so that the resulting preloads on the linkage bearings occur near the middle of the normal operating range. As applied rotor torque increases through the preload level, the loading on some of the linkage bearings is reversed, and bearing friction creates a kink in the strain-gage response curve, as is clearly evident in the figure. The reverse of this kink shows up in almost all other transducer responses, most noticeably for the isolators because the sum of all loads must cancel. Other transducers show this effect with lesser severity because the 2° rotor shaft tilt causes imperfect load sharing and cross-coupling.

These nonlinear responses can be canceled out by a conventional direct regression, but not by an inverse regression. During direct regression, all transducer data must be used together with the applied torque data to properly cancel out the kink in the torque-linkage response. However, this is not possible with an inverse regression, which uses data from only one transducer at a time. Nor can the torque-linkage strain-gage data simply be deleted, because nonlinearities would remain uncanceled in the other transducer data. The

focused load-cell arrangement greatly reduced the problems with highly redundant data that led to the original choice of inverse regression for earlier work (ref. 2). Therefore, direct regressions were used exclusively for this calibration.

The problems associated with the torque linkage would be ideally addressed by rebiasing the preloads for the torque linkage, thereby placing the net preload well outside of the normal operating load range. This option is restricted by requirements of new rotors and flight-test programs, especially compound helicopter tests with low rotor-power settings, and will have to be separately addressed for each individual case. Any adjustments to the torque linkage will necessitate a new calibration.

In addition to the isolators, load cells, and torque linkage transducers, the measurements of isolator piston displacements also were included. Preliminary analysis showed that including displacement data in the regression did not consistently improve the load-measurement errors because of the absence of statistically reliable correlations between piston displacements and applied loads. This result was actually favorable because significant displacements could occur only as a result of a malfunction of the isolator system, which is

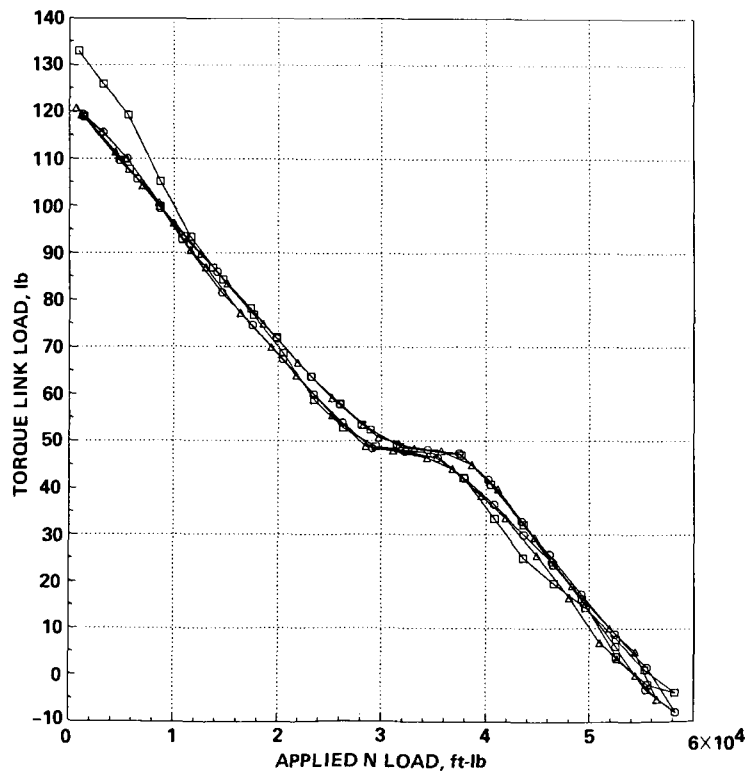


Figure 17.— Torque-linkage strain gage response to applied single N load. (Data point symbols designate different consecutive calibration runs.)

supposed to be self-centering; piston displacements should not be correlated with loads.

Regressions were also run with aft isolator load data included. Again, no consistently significant improvements were noted. This was also a favorable result. The aft isolator was not activated; if including its data had led to any important increase in accuracy, that would have meant it was improperly taking up loads. All displacement data and the aft isolator load data were deleted from all further regression analyses, including those for which results are given in this report.

Regression Results

All data sets used for calibration analysis are listed in table 3, organized by case number. Each case includes a different combination of constant loads in the vertical (Z) and torque (N) axes, with varied loads in other axes. A constant load of zero means that there was no fixed load; varied loads were applied in that axis only. Constant loads were applied in the Z and N axes only. (These are the two axes that, in straight-and-level flight or hover, would experience large constant load components in addition to relatively small trim and vibratory loads.) The different analytical cases were accordingly based on different levels and combinations of constant loads in these two axes, thus simulating different flight conditions.

Three data sets, composing two cases, are of particular importance. Case 1 comprised the single-loads data. In this case, each axis in turn was loaded to its maximum permissible value in each direction (table 1) while all other axes were unloaded. Case 6 was designed specifically to provide two slightly different data sets for multiple-load accuracy references. One data set consisted of 50% Z plus 85% N data, corresponding to maximum-weight hover; the other consisted of 25% Z plus 40% N data, corresponding to an idealized light-weight hover. These two data sets are also appropriate for straight-and-level flight and coordinated turns.

The usual calibration procedure was to hold Z and N constant while loads in other axes were varied one at a time over their maximum allowable ranges (table 1). Calibration data for the Z or N axes had to be separated into individual cases in which one axis (Z or N) was held constant while the other was varied. To achieve complete and consistent data distributions within each case, some data sets were repeated, as shown in table 3.

The first step in the analysis was to calculate the errors resulting from the use of a calibration matrix which was derived directly from design geometry. These errors could be used for comparison with matrices produced by regressions. This is the "geometric" matrix used to calculate the predicted errors of table 2. Its elements are listed in appendix A, and its derivation is given in appendix B. The results of using

TABLE 3.—LOAD COMBINATIONS

Case	Constant loads, % full scale		Varied loads ^a
	Z	N	
1	0	0	X, Y, Z, L, M, N (2 replications)
2	0	85	X, Y, L, M
	25	85	
	50	85	
3	50	0	X, Y, L, M
	50	40	
	50	85	
4	0	0	N
	25	0	
	50	0	
5	0	0	Z
	0	40	
	0	85	
6	25	40	X, Y, L, M
	50	85	

^aFor definitions of variables see table 1.

the geometric matrix were needed to verify the requirement for a full regression analysis, and to provide a worst-case set of errors for comparison.

Three reference data sets were used: single loads, "light hover" (25% Z plus 40% N), and "heavy hover" (50% Z plus 85% N). Table 4 gives the applied-load errors resulting from applying loads in the same axis as that in which loads are measured. For reference, table 4 also gives the overall errors for each axis, calculated by computing the rms error over all applied loads. (The overall errors for single loads in table 4 are the same as those for the geometric matrix given in table 2.) Thus, the overall errors include the effects of all applied loads on a given measurement axis, while applied-load errors include the effect of one load at a time.

Table 5 shows similar errors. However, these errors are calculated for regression matrices derived directly from each respective data set (single loads, light hover, and heavy hover), which results in statistically optimum calibration corrections for each data set. The regression matrices are listed in appendix A, along with the geometric matrix. Plots of responses to applied loads for the three data sets, corrected with matched regression matrices, are given in appendix C.

TABLE 4.— ERRORS FOR THE GEOMETRIC MATRIX^a

Applied-load axis	Data sets		
	Single loads	Light hover	Heavy hover
Applied-load errors			
X, lb	465	357	503
Y, lb	314	192	235
Z, lb	252	139	204
L, ft-lb	820	768	581
M, ft-lb	346	618	703
N, ft-lb	9852	4186	6757
Overall errors			
X, lb	314	196	287
Y, lb	232	164	174
Z, lb	110	55	64
L, ft-lb	992	723	658
M, ft-lb	1064	580	794
N, ft-lb	3489	1776	2832

^aRMS errors for the geometric matrix applied to three reference data sets. Intercepts have been adjusted to give zero mean total errors for each axis in each data set.

The applied-load errors are nearly always lower for the regression matrices (table 5) than for the geometric matrix (table 4). The exceptions are all in roll (*L*) and pitch (*M*), and are not severe. Also, the regression matrices always give better results for overall errors. Note that torque errors are improved by an order of magnitude, compared to those in table 4.

These results were expected: the regression matrices should give better results than the geometric matrix, especially for the overall errors. Furthermore, the overall errors are usually lower than the applied-load errors. Again this was expected because most of the errors that were averaged together resulted from conditions in which no loads were applied to the measurement axis itself. Only severe cross-coupling errors could force the overall errors to be consistently larger than the applied-load errors; even then, proper regressions would correct this. The applied-load errors are, consequently, conservative estimates of measurement-system accuracy.

After the need for regression analysis to derive useful calibration corrections was verified, the requirement for multiple-loads analysis was investigated. Table 6 shows the errors obtained when the single-loads regression matrix was applied to the three reference data sets. The errors obtained for the two hover data sets are greater than those for the single-load data set, and are also greater than those shown in

TABLE 5.— ERRORS FOR THREE REFERENCE DATA SETS^a

Applied-load axis	Data sets		
	Single loads	Light hover	Heavy hover
Applied-load errors			
X, lb	249	213	273
Y, lb	268	175	170
Z, lb	107	84	104
L, ft-lb	737	807	644
M, ft-lb	393	521	564
N, ft-lb	359	320	265
Overall errors			
X, lb	196	129	179
Y, lb	188	148	148
Z, lb	63	33	35
L, ft-lb	806	679	588
M, ft-lb	604	413	492
N, ft-lb	341	209	265

^aResults of using separate regression matrices derived directly from each data set.

TABLE 6.— APPLIED-LOAD ERRORS FOR THE SINGLE-LOADS MATRIX APPLIED TO THREE REFERENCE DATA SETS

Applied-load axis	Data sets		
	Single loads	Light hover	Heavy hover
X, lb	249	321	410
Y, lb	268	217	314
Z, lb	107	159	118
L, ft-lb	737	1315	774
M, ft-lb	393	645	776
N, ft-lb	359	629	471

table 5 for matrices matched to each data set. This indicates that a single-load calibration is inadequate to get good results from normal flight conditions.

The calibration rms errors in table 5 are the same as, or less than, those predicted in table 2 for the majority of axes. When they are greater, they are not excessively so. No rms error in table 5 was greater than 5% of full-scale load in its axis; the important lift and torque errors were less than 1%.

The greatest relative errors are in L , followed by Y (side force). Note that in these two axes, the loads are shared by two isolators, and the load sharing is not uniquely constrained. The N loads are also shared, but the two isolators work with each other to create a torque couple; non-uniqueness is not a problem here. The X (longitudinal force) and M axes have the next highest relative errors, largely because of hysteresis.

The results shown here have a wider range of applicability than may be immediately apparent. The heavy-hover data set is also appropriate for many straight-and-level flight conditions, and the light-hover data are appropriate for similar flight conditions at lower speeds and weights. The light-hover data also apply to the RSRA compound in partially wing-borne flight. The ideal result would be a single matrix which is valid for all reasonable flight conditions. However, this is not realistically obtainable if the highest possible accuracy is required for every flight experiment.

The analysis just presented can be readily expanded to include different reference data sets to match a variety of possible RSRA compound flight conditions. If a more detailed regression analysis is required, the effects of different constant loads can be checked by comparing new combinations of data sets. Either Z or N could be selected at a fixed value while the other axis is set at progressively higher constant loads. The data organization shown in table 3 was chosen in part to readily allow such an analysis for 0-25-50% Z and 0-40-85% N . However, such analyses probably would not be useful because hysteresis is the dominant error mechanism, regardless of loading condition. Accordingly, further analytical efforts were directed toward the problem of hysteresis, as described in the following section.

In addition to these calibration regression errors and hysteresis, it should be noted that other errors occurred (primarily data-system errors). These additional corrections and errors are discussed in the section entitled "Summary of Errors."

ALGORITHM FOR HYSTERESIS REMOVAL

Hysteresis was a major source of residual error; specifically, hysteresis which was caused by static friction in the isolator internal seals and rod-end spherical bearings. Classic hysteresis is evident throughout the figures presented in references 3 and 4. Static friction was also a major contributor to the errors calculated by Madden (see the footnote on page 7). Such errors can be expected to be dithered out in flight by airframe vibrations. This has already been verified for the all-load-cell load-measurement system (ref. 2). For both load-measurement systems, the fundamental causes of error are similar; consequently, the same in-flight behavior may be expected. Furthermore, the isolators reduce vibratory forces at the airframe by absorbing rotor vibrations with small internal displacements. These small motions enhance

the dithering effect. Therefore, for improved predictions of in-flight behavior, it is valid to analytically remove from the calibration data any errors caused by hysteresis. Note that it is not appropriate to attempt to refine the calibration matrix itself because it is already the best linear predictor.

The requirement is to remove the effects of hysteresis on the data without affecting any other statistical properties of the data (biases, slopes, scatter, and mean nonlinear responses). The adjusted data should accurately reflect what would be seen in flight, where hysteresis is dithered out by aircraft vibrations. The presence of other nonlinearities (characterizable by high-order polynomials) complicates the problem. The approach taken here is to find a common polynomial curve fit for both sides of each hysteresis band, then to adjust each side of the band by a constant for a least-squares fit to the common curve.

Hysteresis effects may be removed either from the raw data prior to any regressions, or from the residual errors after calibration corrections. The second approach was taken for several reasons. If hysteresis remains in the raw data for the regression analysis, the regression errors will be rigorously traceable to the National Bureau of Standards. (Removal of hysteresis gives an *estimate* of actual system behavior in flight.) Also, it is often difficult to distinguish between hysteresis and other nonlinearities in the presence of random errors. As was mentioned under "Preliminary Analyses," some nonlinearities can be canceled out in a linear regression. The problem is thereby made more tractable. Moreover, the regression can be used to eliminate low-accuracy transducers on statistical grounds. Finally, the calibration matrix derived by the regression converts a large number of transducer outputs to only six predicted forces and moments. This reduces the amount of data (and the number of computer runs) needed for analysis of hysteresis effects.

The hysteresis corrections were in fact performed on the initial calibration errors; that is, on the differences between the loads predicted by a given calibration matrix and the true calibration loads (fig. 16). This eliminated the dominant linear dependency of predicted loads on applied loads.

General Procedure

The first step of the hysteresis-removal algorithm used here is to separate the errors into upper and lower bands for each subset of calibration data (each of 36 combinations of six applied loads and six responses, one for each axis). This is done by finding a separation line (a polynomial curve fit) that is the best estimate of the error response for each data subset. A nonlinear regression was run for each subset, using all data in the subset. Subsequently, error points above the separation line are assigned to the upper hysteresis band, and error points below the line are assigned to the lower band.

Figure 18 illustrates this part of the procedure. The solid line is the separation line, and upper and lower bands are marked with different open symbols. This figure also shows

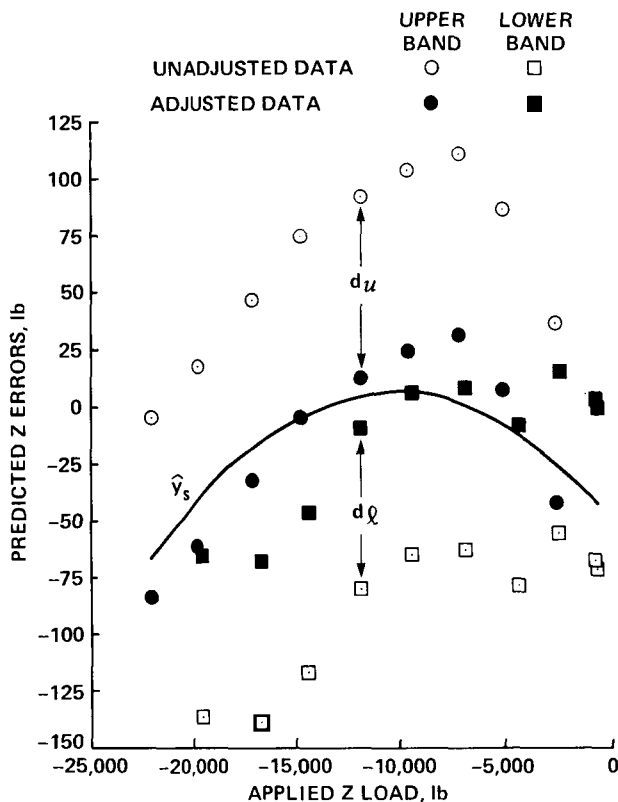


Figure 18.— Application of the hysteresis-removal algorithm to Z-axis errors, showing second-order nonlinearity.

the superposition of hysteresis and a second-order nonlinearity. The separation line must be at least of second order to properly separate the errors, as shown. However, the procedure may fail if the order of the separation-line regression is too great and there are significant random errors. The fitted curve fit may then deviate too far from the center of the true hysteresis band to yield realistic final results. (If the order of the polynomial is the same as the number of error points, a perfect fit could result. Then the separation into hysteresis bands would be determined solely by random numerical round-off errors.)

The separation-line curve fits must allow for residual linear slopes and biases in the error responses. The calibration regression eliminates such errors from the calibration data set as a whole, but some errors may remain in individual subsets of the data. First-, second-, and third-order polynomials were tried on each reference calibration data set, and all results were plotted for inspection as in figure 18. This was necessary because perfect separations are rare, and the choice of order of the separation line is usually a compromise between fitting the nonlinearities and fitting the hysteresis pattern. Several checks on the performance of the algorithm are discussed in the following paragraphs.

After the errors have been separated into upper and lower bands, adjustments can be calculated. The adjustments d_l and d_u shift the data to eliminate the effect of pure hystere-

sis. For the upper band, the equation for the correction constant is

$$d_u = \sum_{i=1}^{n_s} a_i \bar{x}_u^i + b_s - \bar{y}_u \quad (2)$$

with a corresponding equation for the lower band. (The full derivation is given in the next section, Derivation of Correction Constants.) For each band, means are calculated for the error response y_u and for the applied load x_u , up to the maximum order n_s of the separation-line polynomial. These values are then used with the coefficients a_i and intercept b_s of the separation-line regression to calculate the correction constants, which are added to the data points in the corresponding band. The solid symbols in figure 18 are the adjusted data. The rms error is then recalculated using the adjusted error points (see table 7 and the section entitled "Discussion of Results").

Numerical accuracy may become a problem if the order of the separation-line polynomial becomes too large. An accuracy check was always made by calculating the mean correction, which should be zero. No important problems were found through the third order, which was the highest degree of nonlinearity fitted.

If the hysteresis is not large compared to the data scatter in each hysteresis band, the algorithm used here may not properly separate the errors or accurately calculate the correction constants. To guard against such failures, the adjustments for each data subset were tested for statistical significance. For computational convenience, the following test was used. Each hysteresis band was fitted with a third-order polynomial and the two residual rms errors (one for each band) were averaged. The errors in that subset were not adjusted if the sum of the correction constants ($d_u + d_l$) was less than twice the rms average of the residual errors. On average, such a test has a 2.5% chance of improperly permitting adjustments that are in fact determined by random errors instead of by hysteresis. Although not rigorous, this test approximates a 2σ significance test sufficiently for present purposes.

The test used here is not quite the same as that used in reference 4. In that study, the residual errors were simply added together; the resulting test was equivalent to separately testing each adjustment against the residual error in its own hysteresis band, then summing the results. This procedure rejected adjustments too often. The reasoning behind the present method is that the hysteresis is superimposed upon all other errors, and does not contribute to the random errors. Therefore, the residual errors of each hysteresis band are separate samples of the same error; that is, the residual error remaining after hysteresis is removed (as it would be in flight). The significance test should compare the total width of the hysteresis band against the best estimate of the total random error without hysteresis, which is the average of the residual errors in each hysteresis band weighted by the degrees of freedom of the curve fits for each band.

Another change was that of allowing the curve fit to each hysteresis band to be as high as third order, because sometimes the best separation-line polynomial was of a lower order than the best curve fit to one or both bands. Figure 19 shows a subset of data for which a second-order curve fit adequately separates the data into upper and lower bands, but the upper band requires a third-order curve fit to match its response.

Also apparent in figures 18 and 19 is a fundamental problem facing the analysis: the error distribution is not Gaussian, because hysteresis is not a truly random error. Furthermore, upper and lower bands may not have identical responses. In addition, it is possible for an improper separation of hysteresis bands (caused by a separation-line curve fit of the wrong order) to give lower net errors after adjustments than a more realistic separation would give. The choice of curve-fit order cannot be reliably automated because (1) the nonlinearity may not be significant compared to the hysteresis, or (2) the nonlinearity may be statistically significant for one or both hysteresis bands, but not for the complete data subset.

To guard against such problems, all curve fits and adjustments were plotted and inspected. Obvious failures of the algorithm were rejected. This is a completely acceptable procedure because the basic intent of the algorithm is to eliminate the tedium and guesswork of manually separating the

data into hysteresis bands. The algorithm greatly reduces the judgmental aspects of isolator-system error analysis and gives adequate results for estimation of errors in flight.

It was originally hoped that identification of hysteresis bands could be performed by keeping track of the sequence of applied loads and by separating the errors based on the direction of the last change in the load. However, the responses did not always jump immediately into the opposite band upon reversal of the applied load increments, and even one missing or outlying data point could seriously disrupt such a procedure. The separation-line method used here simply proved to be easier to use for the present calibration analysis.

Derivation of Correction Constants

To simplify the following derivation, the true error response (i.e., without hysteresis) is assumed to be linear. The separation line is then the best linear estimate of the true error:

$$\hat{y}_s = m_s x_s + b_s \quad (3)$$

with slope m_s and intercept b_s derived by a linear regression on all of the errors (including both hysteresis bands) remaining after calibration-matrix corrections. At each value of the applied load, x_s , the actual error is compared to the predicted error, \hat{y}_s , and is assigned to one of the two hysteresis bands, y_u or y_l (fig. 18). All data points on either hysteresis band are to be adjusted by a constant, d_u or d_l , matched to each band.

To find the values of d_u and d_l , construct an error function

$$e_u = (y_u + d_u) - (\hat{y}_s) \quad (4)$$

and a similar function for e_l . The requirement is to minimize the total sum of squares

$$\sum e_u^2 + \sum e_l^2$$

with respect to d_u and d_l . The equations for e_u and e_l are completely independent, and partial derivatives may be taken separately:

$$\frac{\partial \sum e_u^2}{\partial d_u} = \frac{\partial}{\partial d_u} \sum_{\text{all } x_u} [y_u + d_u - m_s x_u - b_s]^2 \quad (5)$$

This leads to

$$\sum_{\text{all } x_u} [y_u + d_u - m_s x_u - b_s] = 0 \quad (6)$$

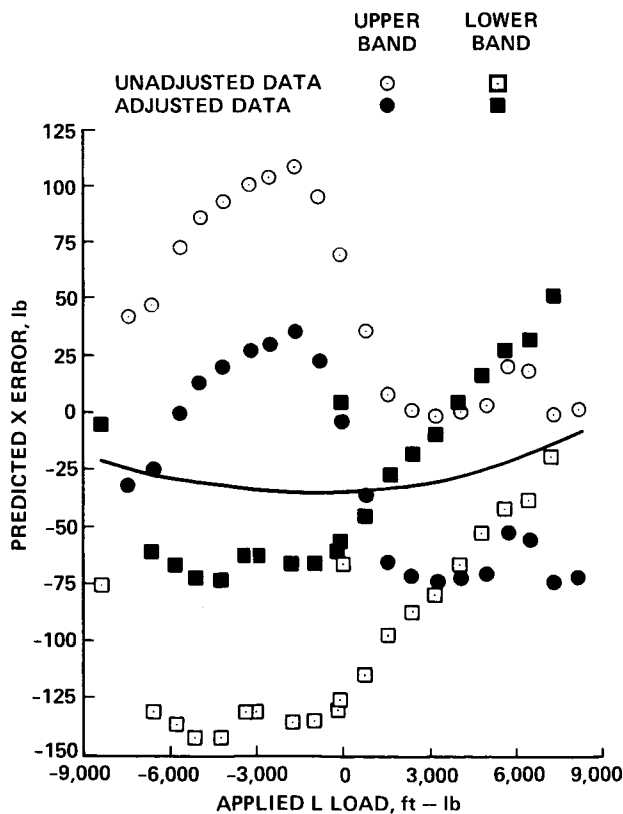


Figure 19.— Application of the hysteresis-removal algorithm, showing second- and third-order nonlinearities.

and, letting n_u equal the number of data points in the upper band,

$$\sum y_u + n_u d_u - m_s \sum x_u - n_u b_s = 0 \quad (7)$$

with similar equations for d_l .

Solving for d_u and d_l ,

$$d_u = m_s \bar{x}_u + b_s - \bar{y}_u \quad (8)$$

and

$$d_l = m_s \bar{x}_l + b_s - \bar{y}_l \quad (9)$$

These equations also satisfy the condition

$$n_u d_u + n_l d_l = 0 \quad (10)$$

That is, the net adjustment to all data in each subset is zero, so that no net bias error is added.

The final result is also quite simple: the data on each hysteresis band are shifted by their average distance from the separation line. The derivation given above shows that this yields the least-squares error, regardless of the mean slopes of each hysteresis band and regardless of the data scatter. Note that if the slopes of the upper and lower bands are exactly equal to the slope of the separation line, the adjustments are simply equal to the differences between the intercepts. Note also that the adjustments have no effect on the calibration

matrices or intercepts. Instead, by removing hysteresis that would not be present in flight, the adjustments improve the estimation of errors which remain after calibration matrix corrections are made.

Extension of the foregoing derivation (eqs. (3)-(10)) to include higher-order polynomials is straightforward, and was used to derive equation (2).

Discussion of Results

Table 7 gives applied-load and overall errors for the two reference data sets, with and without adjustments for hysteresis. The values for unadjusted errors are the same as those in table 5. Errors in three axes are significantly reduced (by about one-half for M , a little less so for X , and somewhat more so for Z). In two axes, Y and L , application of the hysteresis-removal algorithm caused moderate reductions in error; relative to the total, the reductions were greater for Y than for L . The algorithm had no effect on N for the heavy-hover data, and only a modest effect on N for the light-hover data. For overall errors, the net result of applying the algorithm was a moderate (less than 50%) reduction of error for virtually all axes of both data sets.

Hysteresis does not appear to contribute significantly to errors in the lateral axes, especially N , but it is possible that hysteresis is being masked by other errors. The regression analysis cancels out known nonlinearity in the torque-linkage response as well as is possible, but cancellation cannot be per-

TABLE 7.—EFFECTS OF THE HYSTERESIS-REMOVAL ALGORITHM ON THE TWO REFERENCE DATA SETS

Applied-load axis	Light-hover data		Heavy-hover data	
	Unadjusted	Adjusted	Unadjusted	Adjusted
Applied-load errors				
X , lb	213	115	273	146
Y , lb	175	125	170	106
Z , lb	84	38	104	35
L , ft-lb	807	712	644	493
M , ft-lb	521	272	564	273
N , ft-lb	320	221	265	265
Overall errors				
X , lb	129	77	179	103
Y , lb	148	105	148	97
Z , lb	33	23	35	17
L , ft-lb	679	457	588	443
M , ft-lb	413	280	492	282
N , ft-lb	209	152	265	229

fect, or even consistent, over all applied load combinations. Moreover, this may result in unevenly overlapped hysteresis contributions from each transducer. (That is, hysteresis errors from each of 16 rod ends plus the torque linkage itself may not be evenly distributed or evenly weighted in the resultant load errors.) The residual nonlinearity may be of too high an order, and the total errors too far deviated from pure hysteresis, to make reliable corrections for even major hysteresis errors.

It is possible to preload the torque linkage such that the nonlinear region of the response lies largely outside the range of practical flight loads. This should be attempted during the next calibration to determine whether this is the major cause of system nonlinearity, and to see whether the errors fall evenly into a classic hysteresis response. Of course, if the errors are due to other causes, such as non-unique load sharing between the two lateral isolators, then rebiasing the torque linkage will not eliminate such errors.

The actual choice of a calibration matrix would depend upon both the errors in table 7 and the actual flight conditions. Obviously, the matrix should match the gross weight (light or heavy), but there would be a choice at intermediate or varying weights. Based on errors in Z or N , there is little choice between the light- and heavy-hover matrices. However, applied-load errors in L , for example, could be improved significantly if the flight data were, in fact, being collected at high gross weights. Estimates of X , on the other hand, would be improved by using the light-hover matrix when flight conditions permit.

SUMMARY OF ERRORS

Table 8 summarizes the different errors affecting load measurement accuracy. Calibration reference errors are

determined by the inherent accuracies of the calibration-facility load cells. (Rearrangement of the load cells resulted in net errors which were different from those achieved during the calibration of the compound RSRA as reported in ref. 2.) Regression errors, adjusted for hysteresis, were taken from table 7 and averaged over the light-hover and heavy-hover reference data sets.

Aircraft data-system errors are introduced by aircraft electronics and postflight data processing. To minimize these errors, each data channel was separately calibrated, and the results were converted to equivalent net rotor loads. The electronics and data processing can be optimized for different types of flight tests; the values given in table 8 are averages, meant to illustrate typical performance.

A few words of explanation are in order regarding inertial effects. As the RSRA maneuvers, gravity plus body accelerations act on the mass of the transmission and the rotor head to create inertial loads. These must be calculated and subtracted from the total measured loads to get the true rotor aerodynamic loads. Errors in the calculated inertial loads are caused by errors in the instrumentation used to determine aircraft attitude and acceleration. The inertial effects errors in table 8 are the same as those listed in reference 2, which describes at length the calculation of inertial loads for the RSRA. (The inertial effects are not identical for the two RSRA, but the differences in the error contributions are negligible.)

The rms sum of all errors is given separately for each axis in the last column of table 8. The calibration reference errors and the analytical predictions (regression results) are not strictly independent; the summation used here is more conservative than simply ignoring the facility errors. Note in particular that the analytical prediction is less than the calibration reference error for the Z (lift) axis. The calibration itself is the limiting factor for usable Z -axis accuracy. In all other axes, the effects of the calibration reference errors are negligible.

TABLE 8.—SUMMARY OF LOAD-MEASUREMENT RMS ERRORS

Applied-load axis	Errors				Rms sum of errors
	Calibration reference	Regression (adjusted) ^{a,b}	Aircraft data system ^b	Inertial effects	
X , lb	13	131	18	17	133
Y , lb	11	115	19	10	118
Z , lb	47	36	30	2	66
L , ft-lb	42	603	105	15	614
M , ft-lb	50	272	101	26	296
N , ft-lb	25	243	47	10	249

^aRegression results, adjusted to remove hysteresis.

^bAverage of results for light- and heavy-hover data.

In two axes, Z and N (lift and torque), the total errors are 0.5% (or less) of the design full-scale load ranges. This approaches the accuracy of a good large-scale wind tunnel balance. In two other axes, X (longitudinal force) and M (pitching moment), the total errors are 1.5% (or less), which is also good for such a complex system. In the remaining two axes, Y (side force) and L (rolling moment), the errors are about 2% and 4%, respectively.

IMPROVEMENTS AND FUTURE OPTIONS

It is known that a major error mechanism is hysteresis (ref. 3). Furthermore, test flights with the other RSRA have shown that hysteresis resulting from rod-end bearing friction is largely dithered out by airframe vibration (ref. 2). Consequently, the load-measurement system has measurement accuracy potential beyond that demonstrated here.

It is apparent that a major increase in analytical effort is required for a modest change in predicted accuracy. (The improvements shown in table 7 for hysteresis removal are much less than those shown in tables 4 and 5 for the original multiple linear regression analysis.) A nonlinear regression, possibly in combination with the hysteresis-removal algorithm, would be the next logical step in an extended analysis. For best results, hysteresis should be removed from the raw data before a nonlinear regression is performed. Otherwise, the regression may not be able to properly derive high-order coefficients if the errors contributed by hysteresis are large compared to other nonlinearities. However, this approach would compromise traceability of the data to the National Bureau of Standards by adjusting raw data before calibration coefficients are derived.

A more promising undertaking would be to change the torque-linkage preload to reduce inherent system nonlinearity, or at least to place the region of nonlinearity well outside the range of realistic flight loads. A more elaborate improvement would be to replace with elastomeric units the existing rod-end bearings on the load cells, isolators, and torque linkage, thereby directly removing a major source of hysteresis. It is not likely that off-the-shelf elastomeric bearings suitable for direct substitution would be available. Consequently, such a conversion would entail at least a modest development and qualification effort, plus a full re-calibration.

Improvements are possible in the isolators themselves. It is strongly desired that the active isolators not be rebuilt internally. Doing so would be in violation of the original design philosophy that the isolation system be sufficiently adjustable to accommodate virtually any conventional rotor system without major modification. Moreover, it would be expensive and require complete system requalification. However, a few simple changes easily can be made. For example, the pressure transducers are significantly less accurate than the vertical load cells; direct substitution of improved transducers is an

available option. Also, it was always envisioned that servo-valve feedback gains and accumulator working pressures would occasionally be changed to accommodate new testing requirements.

Improvements to the calibration equipment are already being implemented. The most important change is a more capable data acquisition system which can take much more data, partly because of higher speed and partly because of a greater degree of automation. More data will make replicated data sets possible for all load combinations, thereby allowing errors to be calculated from a replication different from that used to derive calibration coefficients. This would provide greater flexibility and increased statistical rigor in the analysis.

CONCLUSIONS

Whether the RSRA active-isolator load-measurement system could accurately measure static rotor loads was a major unanswered question during the aircraft's development; the reduction of vibrations had already been demonstrated. The first static calibration of the system showed that it is capable of meeting and even exceeding most performance predictions. Calibration corrections based solely on design geometry are inadequate, especially for torque measurements. A regression analysis is required to achieve acceptable results. Furthermore, corrections based on single-load data are significantly different from those derived from multiple-load data sets. Since the latter more closely match actual flight conditions, this result shows that a multiple-load calibration is needed for deriving realistic corrections.

It was also found that errors which were based on loads applied solely in the measurement axis provide conservative estimates of system accuracy, compared to errors which were found by averaging all applied loads. A method of removing hysteresis errors was developed and applied to obtain error predictions more representative of actual flight conditions, where hysteresis is known to be reduced by airframe vibrations. That method was effective (in varying degrees) in all axes but torque, where other errors dominate.

The results are encouraging, and indicate that system measurement accuracy can be improved by straightforward, low-risk component upgrades. The RSRA active-isolator system can control rotor-induced vibrations and can simultaneously measure the six rotor loads on a routine research basis.

Ames Research Center

National Aeronautics and Space Administration
Moffett Field, California 94035

August 19, 1986

APPENDIX A

MATRICES FOR CALIBRATION

This appendix presents four calibration matrices. The first is the geometric matrix, derived directly from the load-measurement system assembly drawings. The other three matrices are derived by regression analyses performed on three data sets: single loads, light-hover triple loads, and heavy-hover triple loads. Regression intercepts are given for the three regression matrices. Use of the matrices $[C]$ and vectors (L) , (B) , and (F) given here is defined in equation (1) in the main body of this paper.

Input vectors (L) for all matrices are the same. Such data vectors are made up of outputs from each transducer, in the following order with the units specified:

Forward load cell	(Fwd LC),	lb
Right load cell	(Rt LC),	lb
Left load cell	(Left LC),	lb
Aft load cell	(Aft LC),	lb
Torque linkage	(Link),	lb

Left isolator	(Left I),	psi
Right isolator	(Rt I),	psi
Forward isolator	(Fwd I),	psi

See figure 4 for the locations of the transducers.

Intercept vectors (B) and output vectors (F) give loads in the following order with the units specified:

X , lb
Y , lb
Z , lb
L , ft-lb
M , ft-lb
N , ft-lb

(See figure 1 for the definitions of the forces X , Y , Z and moments L , M , N .)

The geometric matrix is:

	Fwd LC	Rt LC	Left LC	Aft LC	Link	Left I	Rt I	Fwd I
X	0.2242	-0.03376	-0.03668	-0.2952	0	0	0	-17.309
Y	0	0.2539	-0.2632	0	0	17.320	-17.320	0
Z	-0.9745	-0.9666	-0.9641	-0.9554	0	0	0	0.6045
L	0	-2.915	2.953	0	-0.4741	-81.191	83.254	0
M	2.879	-0.2200	-0.2194	-3.336	0	0	0	-75.106
N	0	0.04399	-0.04320	0	-13.579	28.471	30.611	0

(The intercept vector does not apply to the geometric matrix.)

The single-loads matrix is:

	Fwd LC	Rt LC	Left LC	Aft LC	Link	Left I	Rt I	Fwd I
<i>X</i>	0.1900	0.00263	-0.03827	-0.2520	7.833	1.902	-0.00387	-16.985
<i>Y</i>	0.06564	0.1329	-0.2928	0.1163	-5.354	16.068	-16.107	0.4602
<i>Z</i>	-0.9700	-1.0017	-1.0126	-0.9420	4.065	0.7845	0.5408	0.6787
<i>L</i>	-0.3725	-2.352	3.154	-0.5143	16.448	-77.010	78.273	0.01305
<i>M</i>	2.806	-0.01641	0.09796	-3.514	16.181	1.143	1.128	-78.381
<i>N</i>	0.1332	-0.09717	-0.1948	0.3144	-162.718	28.366	30.424	1.878

Its intercept vector is:

<i>X</i>	-1297
<i>Y</i>	683
<i>Z</i>	-3549
<i>L</i>	-1688
<i>M</i>	-3317
<i>N</i>	9478

The light-hover matrix is:

	Fwd LC	Rt LC	Left LC	Aft LC	Link	Left I	Rt I	Fwd I
<i>X</i>	0.2794	-0.08819	-0.1142	-0.1348	-3.881	1.090	-0.1401	-18.126
<i>Y</i>	-0.02207	0.2248	-0.1640	-0.08955	7.350	16.277	-15.226	-0.1586
<i>Z</i>	-1.0318	-0.9322	-0.9239	-1.0160	-0.07615	-0.4270	0.1684	0.9280
<i>L</i>	0.03060	-2.776	2.686	0.2656	-22.232	-75.388	74.387	1.081
<i>M</i>	3.089	-0.1168	-0.03906	-0.03464	-15.850	0	-1.533	-84.085
<i>N</i>	-0.1394	0.1476	-0.1072	0.04555	-152.114	31.563	28.052	4.735

Its intercept vector is:

<i>X</i>	148
<i>Y</i>	-756
<i>Z</i>	-2655
<i>L</i>	2545
<i>M</i>	723
<i>N</i>	7947

The heavy-hover matrix is:

	Fwd LC	Rt LC	Left LC	Aft LC	Link	Left I	Rt I	Fwd I
<i>X</i>	0.4699	-0.3369	-0.4055	0.1579	-5.011	2.828	0.2645	-19.138
<i>Y</i>	-0.1371	0.1710	-0.1655	-0.03195	3.892	15.766	-15.339	0.3581
<i>Z</i>	-1.0135	-0.9408	-0.9204	-1.0199	-1.441	-0.7462	0.1417	0.4353
<i>L</i>	-0.3400	-2.137	3.171	-0.4943	-12.659	-75.179	70.854	-1.442
<i>M</i>	3.415	-0.4726	-0.5369	-3.046	-14.605	7.172	-3.387	-86.366
<i>N</i>	-0.8687	1.2417	0.9221	-1.1409	-122.925	29.770	24.227	6.177

Its intercept vector is:

<i>X</i>	-325
<i>Y</i>	-101
<i>Z</i>	-2316
<i>L</i>	2685
<i>M</i>	-1163
<i>N</i>	7401

APPENDIX B

DERIVATION OF THE GEOMETRIC MATRIX

Calculation of the geometric matrix was performed by a simple static analysis. The torque linkage was analyzed separately from the rest of the isolator system, assuming that linear superposition holds for the entire system.

Figure B1 is a schematic of the load measurement system, but without the torque linkage. The aft isolator was also deleted because it does not normally react any forces or contribute to load measurements. The system is statically indeterminate; however, by simply summing the load cell and isolator applied forces, the net loads at the rotor head can be derived. Equations are given immediately below. Note that all four load cells are inclined 15° from the vertical.

$$X' = -I_1 + (L_1 - L_2)\sin \alpha \quad (\text{B1})$$

$$Y' = I_1 - I_3 - (L_3 - L_4)\sin \alpha \quad (\text{B2})$$

$$Z' = -(L_1 + L_2 + L_3 + L_4)\cos \alpha \quad (\text{B3})$$

$$L' = -(I_2 - I_3)(a + e) - (L_4 - L_3)C_1 \quad (\text{B4})$$

$$M' = -I_1(a - f) + L_1C_2 + L_2C_3 - (L_3 + L_4)d \cos \alpha \quad (\text{B5})$$

$$N' = I_2c + I_3(h + d) + (L_3 - L_4)d \sin \alpha \quad (\text{B6})$$

where

$$C_1 = a \sin \alpha + b \cos \alpha$$

$$C_2 = g \cos \alpha + a \sin \alpha$$

$$C_3 = (h + d)\cos \alpha - a \sin \alpha$$

α = load cell cant angle

For simplicity, these equations assume a rotor-head coordinate system aligned with the plane of the load-measurement system, denoted by primed axis symbols. To these equations, sine and cosine corrections must be added to account for the 2° forward tilt of the main rotor shaft. Also, various deviations from design specifications (most noticeably in the load cell inclinations) necessitate minor changes in several individual terms of the equations. All such corrections have been incorporated into the geometric matrix given in appendix A.

The torque linkage is shown schematically in figure B2. Angles and offsets have been exaggerated for clarity. The seven members (two lateral restraining links, one longitudinal restraining link, two identical bellcranks, the transmission

subframe, and the airframe) have eight pivot points (three per bellcrank, plus one at the airframe end of each lateral restraint). The longitudinal link is strain gaged to measure its tension F_t .

The isolators (not shown) connect the subframe to the airframe. They are, in effect, extensible links. If they fail to operate, they do not then affect the behavior of the linkage. This is the critical design condition for the linkage. When the isolators are operating, torque loads are shared with the linkage. The torque linkage is preloaded in compression, so that at maximum torque it carries little load. The following analysis assumes superposition of linkage, isolator and load-cell loads, so that linkage loads may be computed separately.

Only very small motions (± 0.21 in.) are allowed by the isolators. Consequently, the inequality of the lengths of the two lateral restraints may be ignored in the simple explanation here. Furthermore, the longitudinal linkage alignment angle Θ is very small, and may be temporarily neglected. For fore-and-aft motions, the bellcranks are (approximately) fixed with respect to the subframe, and the lateral links act as two opposite arms of a parallelogram. For side-to-side motions, the bellcranks pivot in unison, with the lateral restraints remaining straight. In either case, the subframe moves freely with respect to the airframe, without any imposed torques.

If a transmission torque load is applied to the linkage by the subframe, it is felt as a torque couple T_1 and T_2 at the two bellcranks. The bellcranks attempt to pivot in opposite directions, but are restrained by the longitudinal restraining link. The lateral links are loaded by the leverage of the bellcranks and transfer the applied torque couple to the airframe. The subframe does not pivot with respect to the airframe.

Taking moment balances about the lateral link bearings on the bellcranks, and noting that the longitudinal link tension F_t is the same at both ends:

$$\text{left bellcrank:} \quad -T_1k_1 + F_tk_2 = 0 \quad (\text{B7})$$

$$\text{right bellcrank:} \quad T_2k_1 - F_tk_2 = 0 \quad (\text{B8})$$

Adding equations and eliminating k_1 yields

$$T_1 = T_2 \quad (\text{B9})$$

Also,

$$T_1 = T_2 = N'/k_3 \quad (\text{B10})$$

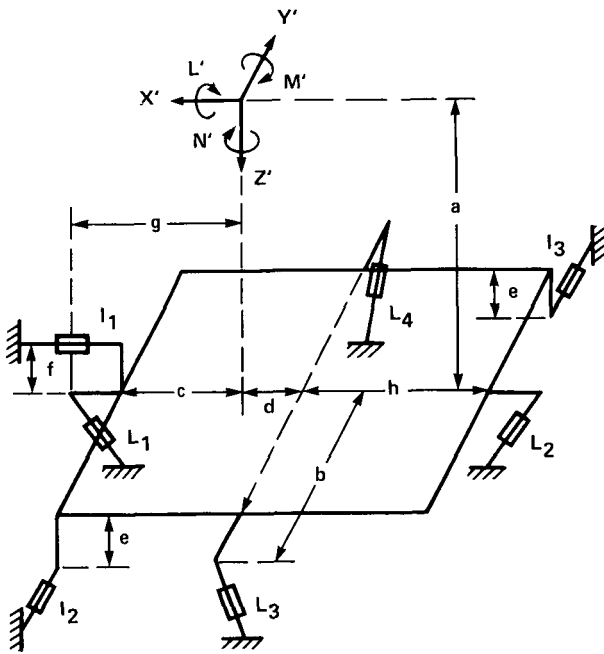


Figure B1.— Layout of the active-isolator load-measurement system. (The torque linkage is shown separately in figure B2.)

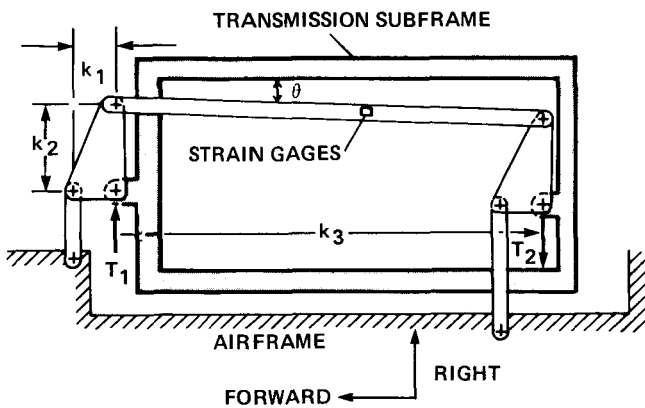


Figure B2.— Schematic at the torque linkage, looking down.

where N' is a torque applied parallel to the plane of the linkage. Substituting for T_1 in equation (B7) and rearranging:

$$N' = F_l k_2 k_3 / k_1 \quad (\text{B11})$$

Equation (B11) gives the value of torque reacted by the linkage, independently of the torque reacted by the isolators and load cells. It can be refined by correcting for the non-parallelism of the longitudinal linkage:

$$N' = F_l k_2 k_3 / k_1 \cos \Theta \quad (\text{B12})$$

Finally, to get loads in the rotor head axis system, N' must be adjusted for the 2° shaft tilt, and the resulting terms for N and L must be added to the geometric matrix. (The matrix shown in appendix A also reflects a sign reversal in the torque-linkage strain-gage output, visible in figure 17.) Further refinements to account for the lateral offsets of the bellcranks are possible, but the changes in the matrix elements are negligible.

The large torque errors found for the geometric matrix (table 4 in reference 4) prompted a re-evaluation of the torque linkage; the analysis given above is a summary of the revised version. The revised geometric matrix gave noticeably different results for torque and roll load-prediction errors (table 2 and figure 15 in the main body of this paper), but there was no net improvement; some predictions actually were worse.

A broader look at the problem shows that large errors are probably inevitable. Adding the load cells and isolators makes the system statically indeterminate. Moreover, the isolators are not linearly elastic: under changing loads, the servo valves are continually changing hydraulic pressures inside the isolators, and small internal leakages prevent the pressures from remaining perfectly constant for repeated loads. A comprehensive analysis is quite beyond the scope of this paper and would have questionable chance of accomplishing a significant improvement, given the large number of uncertainties (e.g., individual servo-valve tolerances). A regression analysis, however, avoids such problems completely, so the major analytical effort was directed there.

APPENDIX C

CORRECTED RESPONSES TO CALIBRATION LOADS

The responses to calibration loads of three reference data sets (for single loads, light-hover triple loads, and heavy-hover triple loads) are shown in figures C1 through C18. All responses have been corrected with regression matrices derived directly from each respective data set. The matrices are given in appendix A. No adjustments for hysteresis errors have been made for these plots.

In each figure, the predicted loads in each axis are plotted against one applied load. For the light-hover data, lift (Z) and torque (N) were held constant at 25% and 50% of full-scale

load, respectively, except where either Z or N itself was defined as the applied load. For the heavy-hover data, the constant values for Z and N were 50% and 85%. Full-scale load values are listed in table 1.

All data have been normalized and plotted as percentages of full-scale loads in the relevant axes. Perfect responses would either follow the applied loads exactly (along the dashed diagonal reference lines), or lie on straight horizontal lines for zero or constant loads.

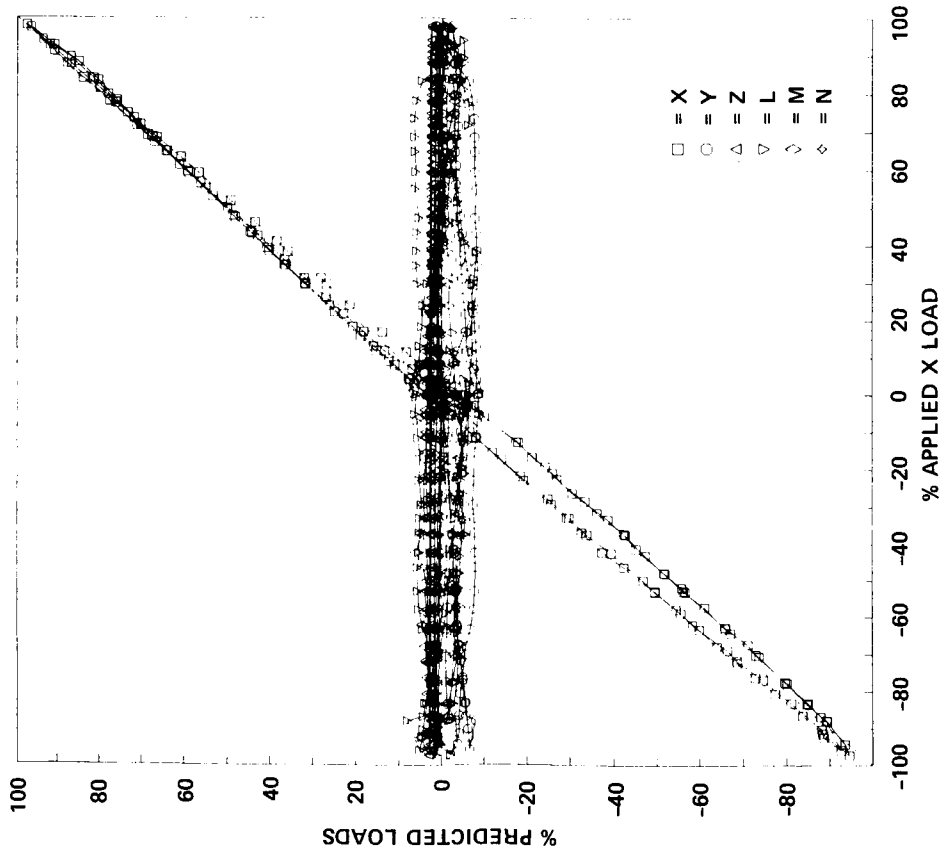


Figure C1.— Responses to applied X load (single loads).

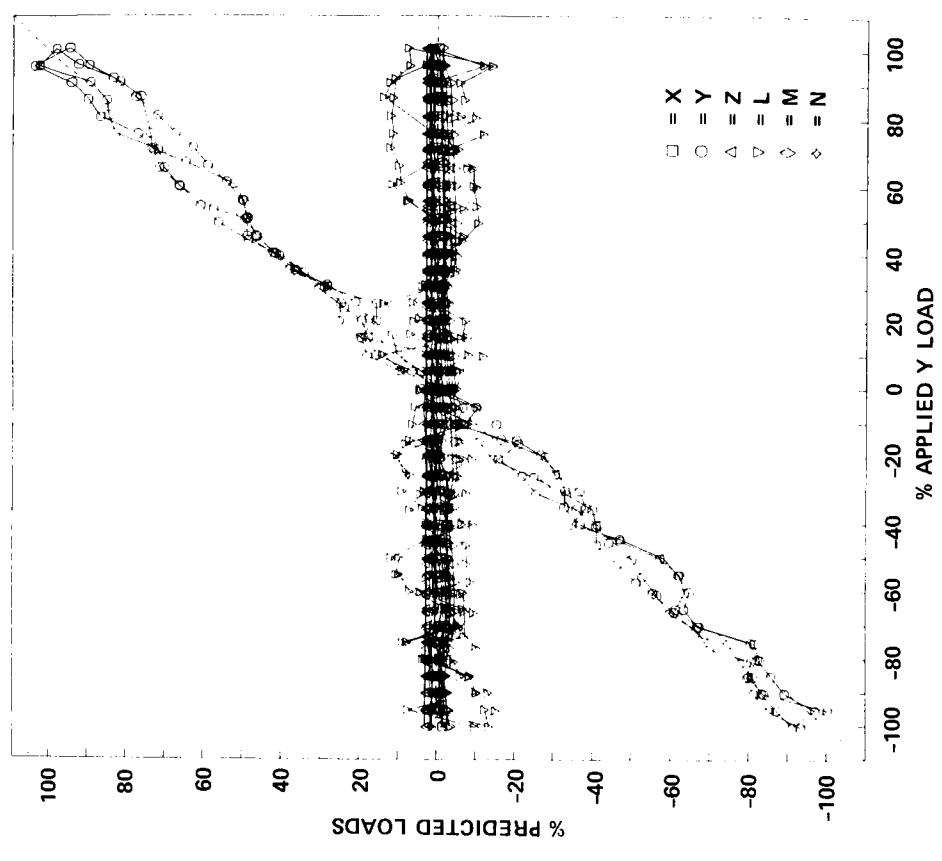


Figure C2.— Responses to applied Y load (single loads).

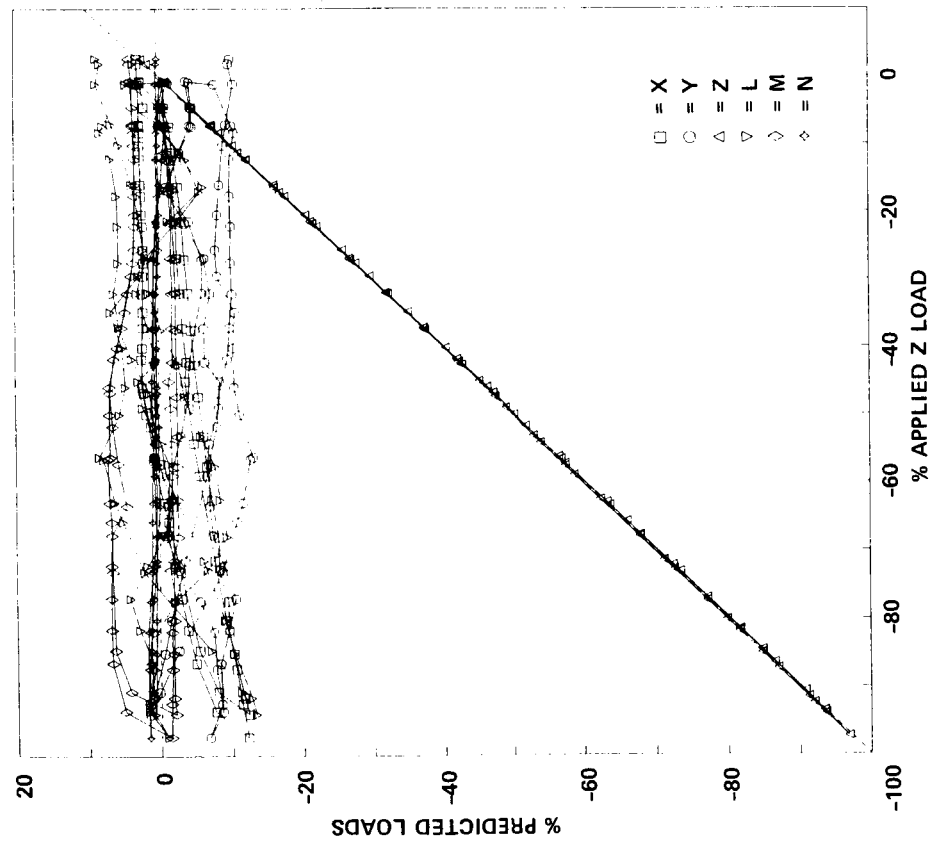


Figure C3.— Responses to applied Z load (single loads).

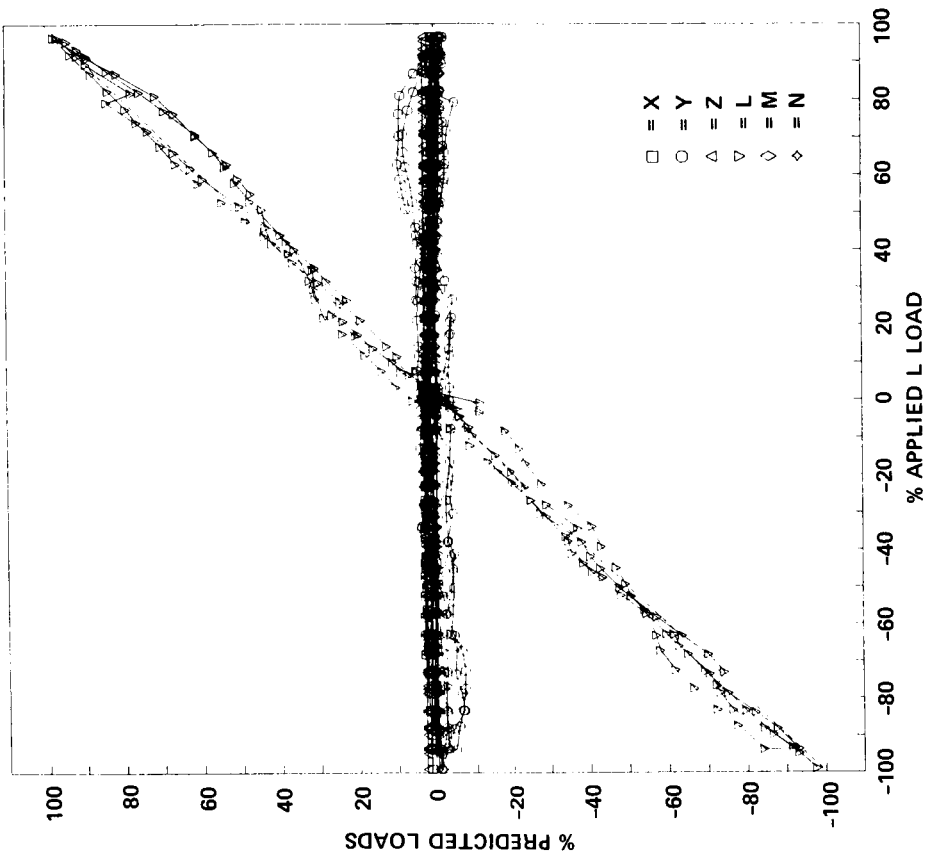


Figure C4.— Responses to applied L load (single loads).

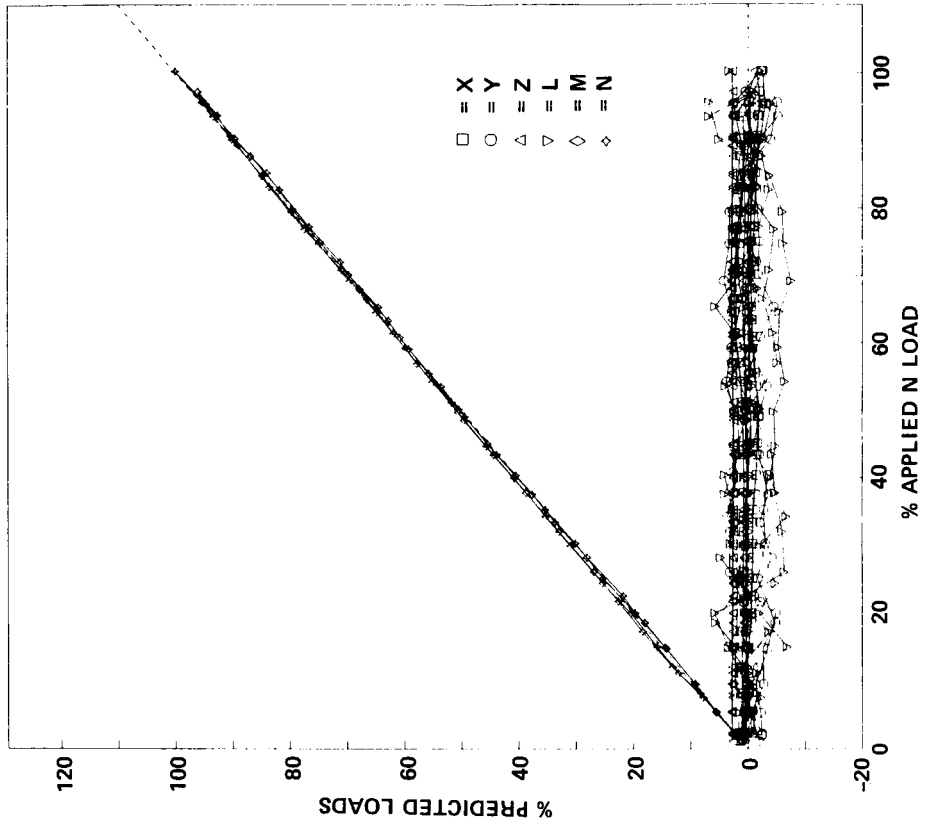


Figure C5.— Responses to applied *M* load (single loads).

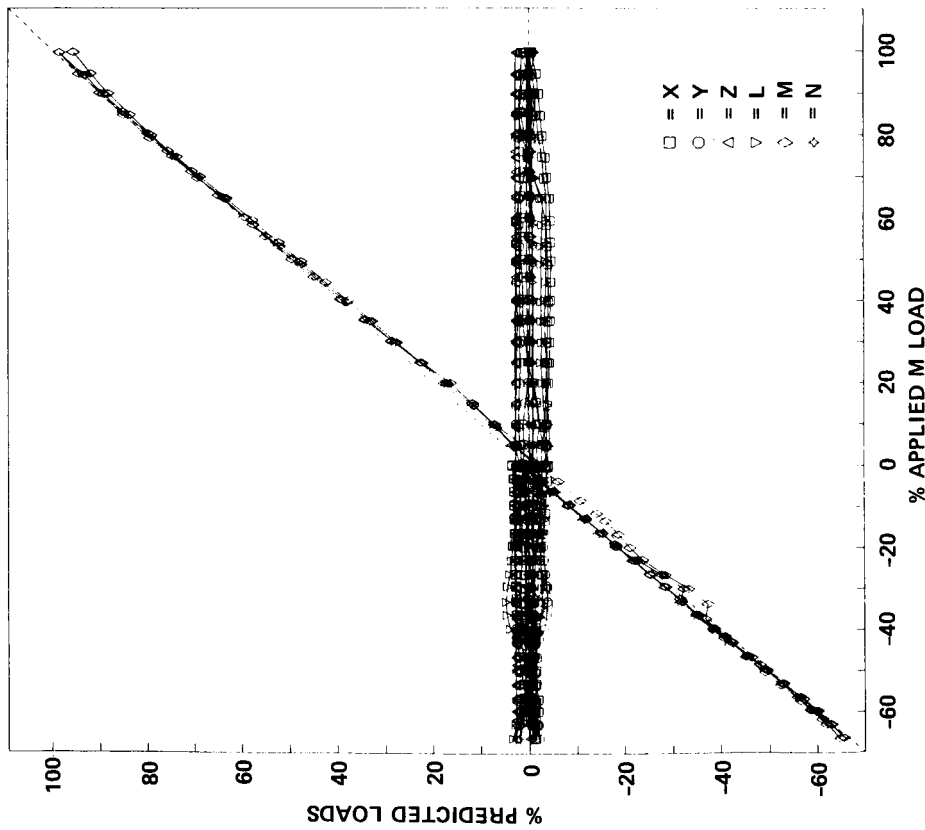


Figure C6.— Responses to applied *N* load (single loads).

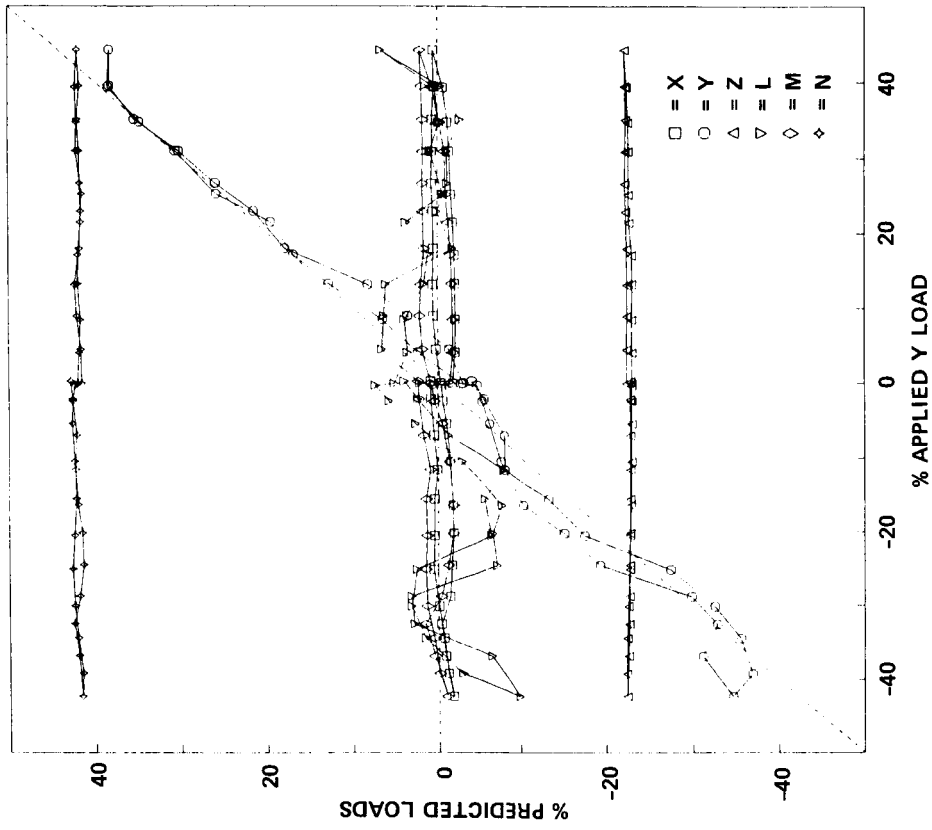


Figure C7.— Responses to applied X load (light-hover triple loads).

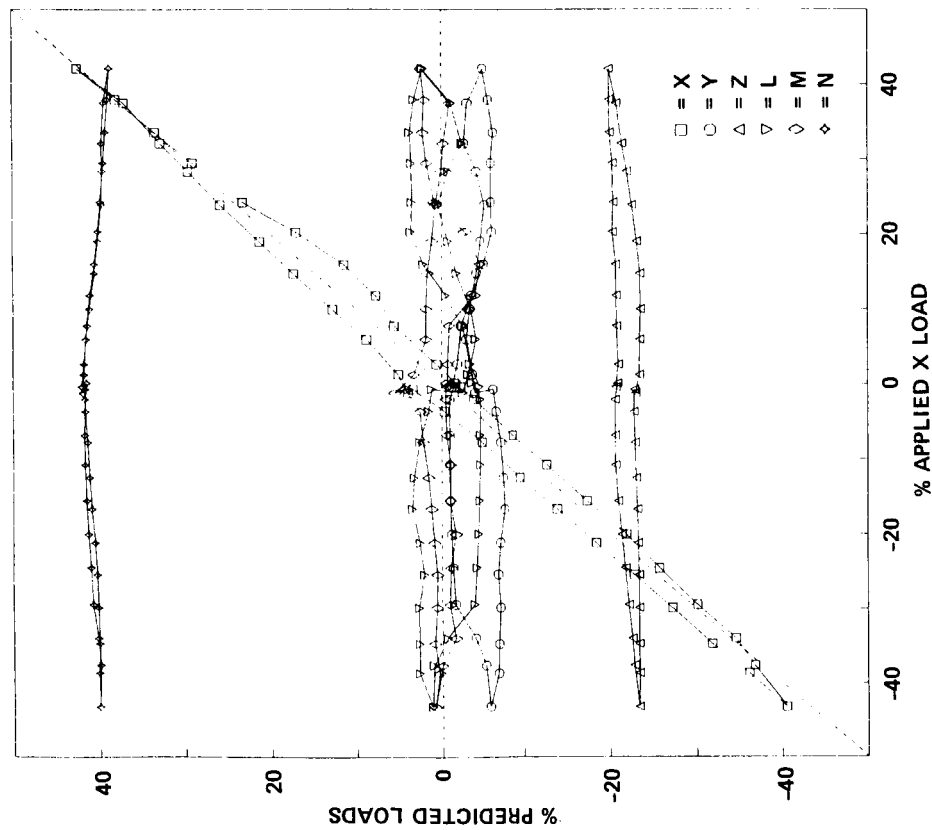


Figure C8.— Responses to applied Y load (light-hover triple loads).

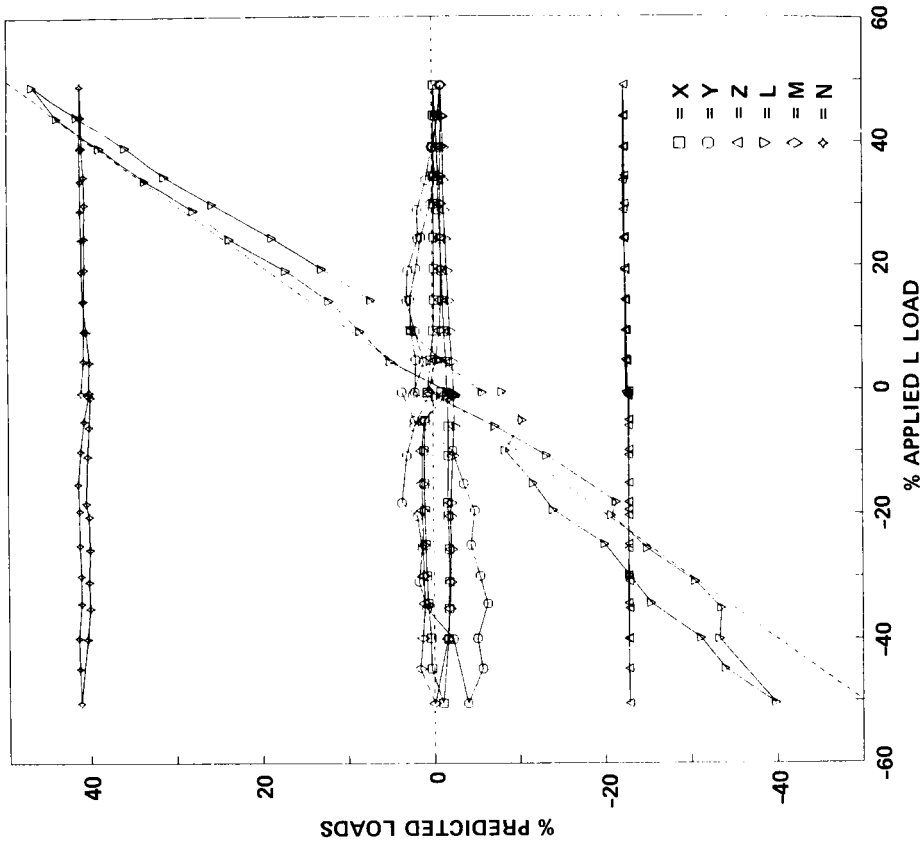


Figure C10.— Responses to applied L load (light-hover triple loads).

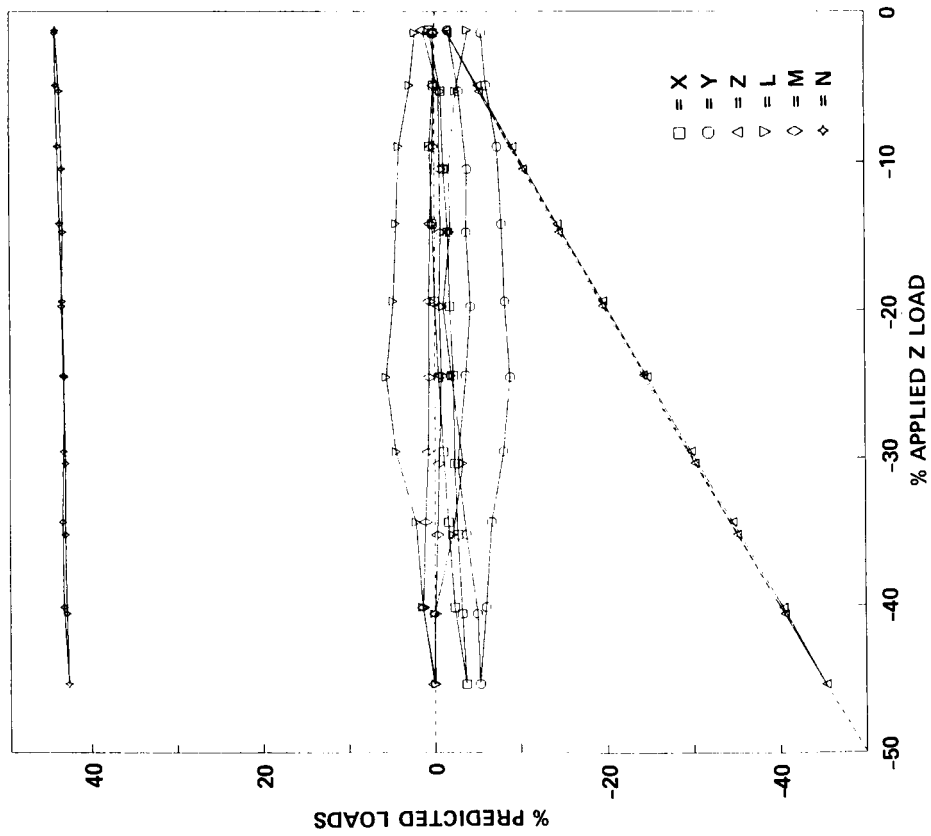


Figure C9.— Responses to applied Z load (light-hover triple loads).

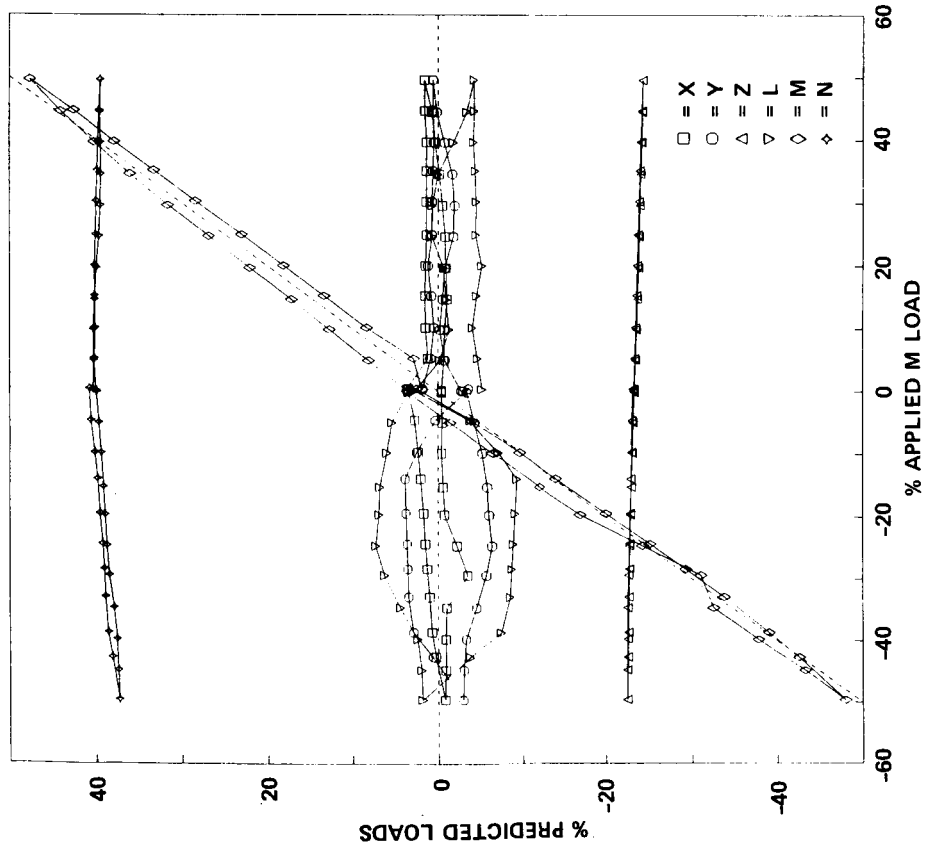


Figure C11.— Responses to applied *M* load (light-hover triple loads).

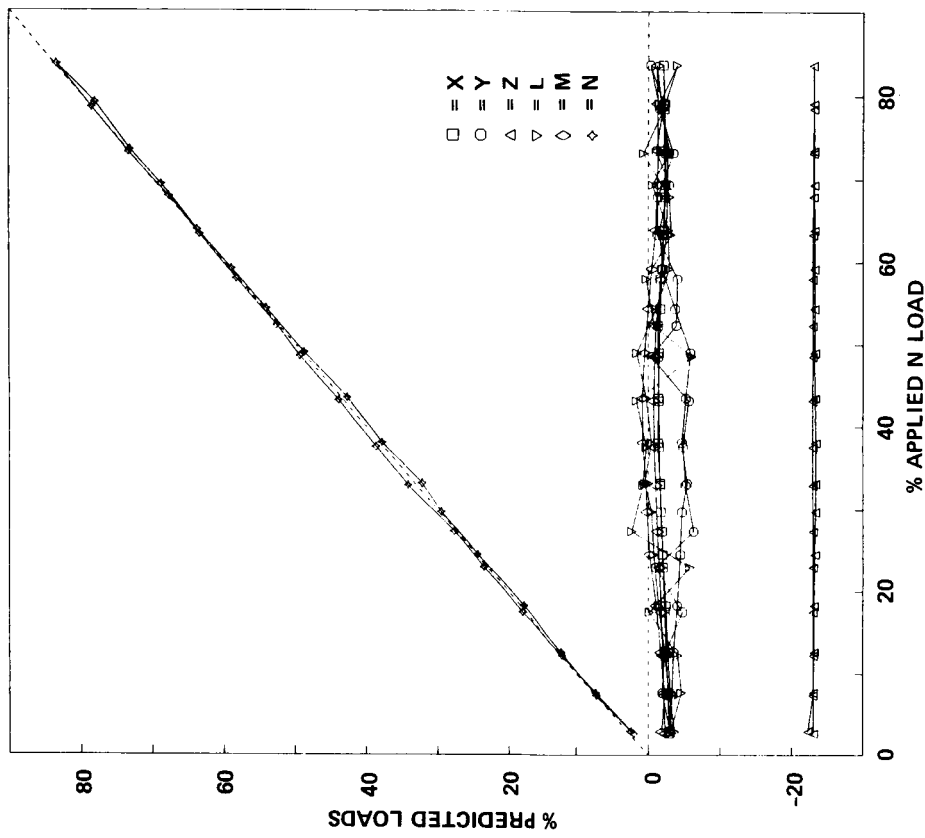


Figure C12.— Responses to applied *N* load (light-hover triple loads).

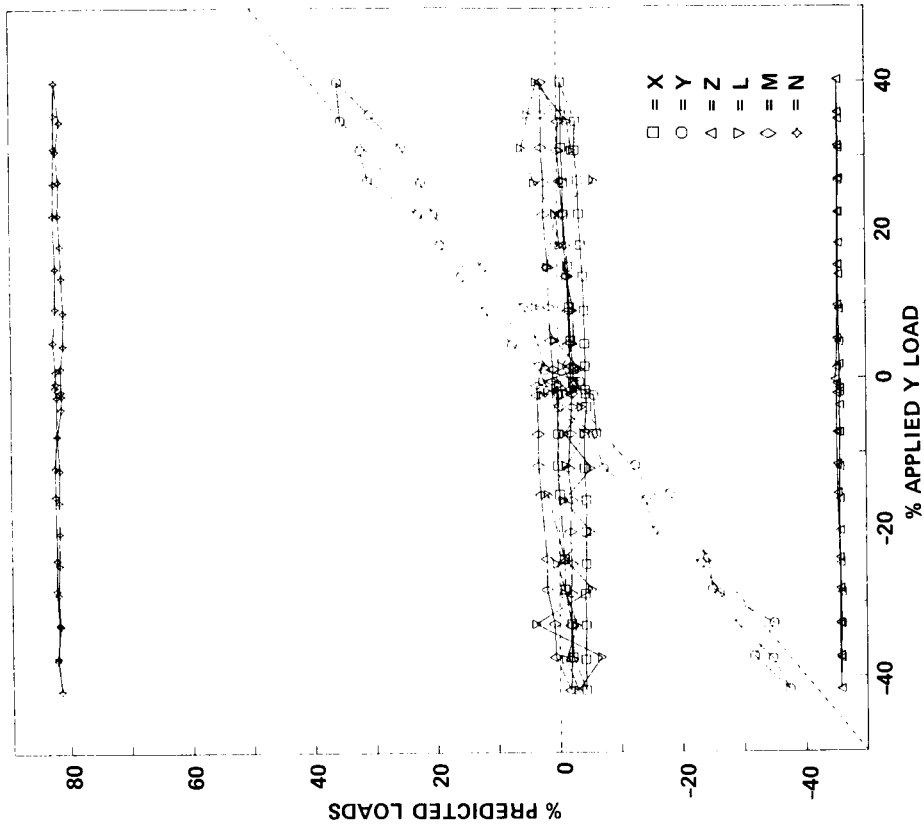


Figure C13.— Responses to applied X load (heavy-hover triple loads).

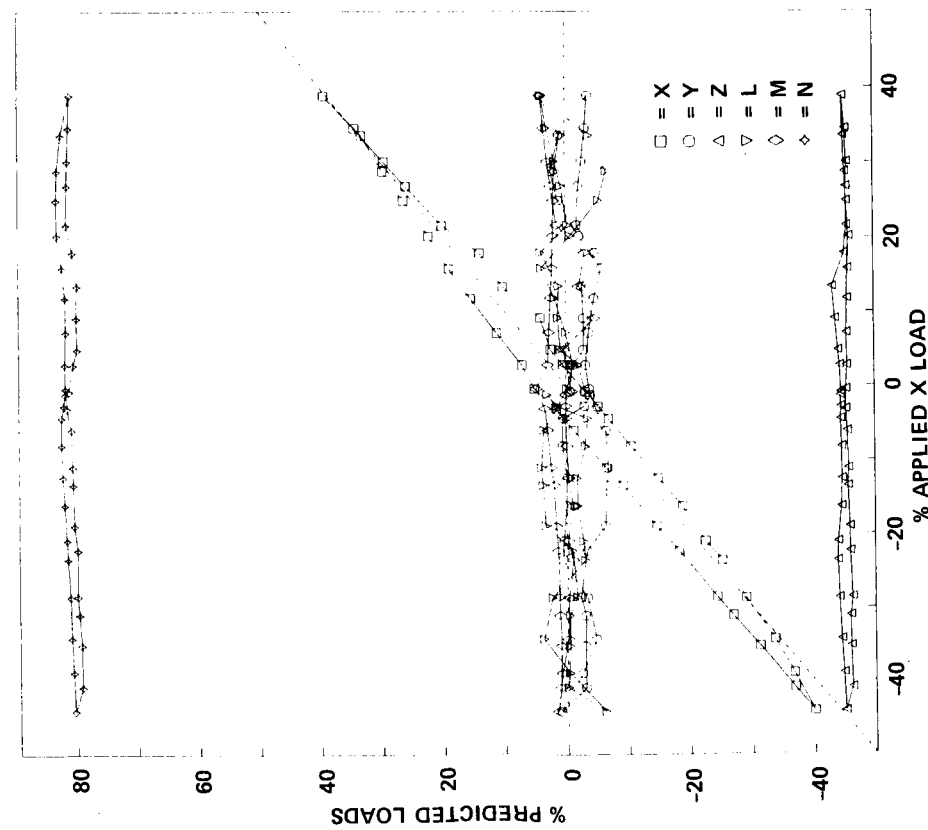


Figure C14.— Responses to applied Y load (heavy-hover triple loads).

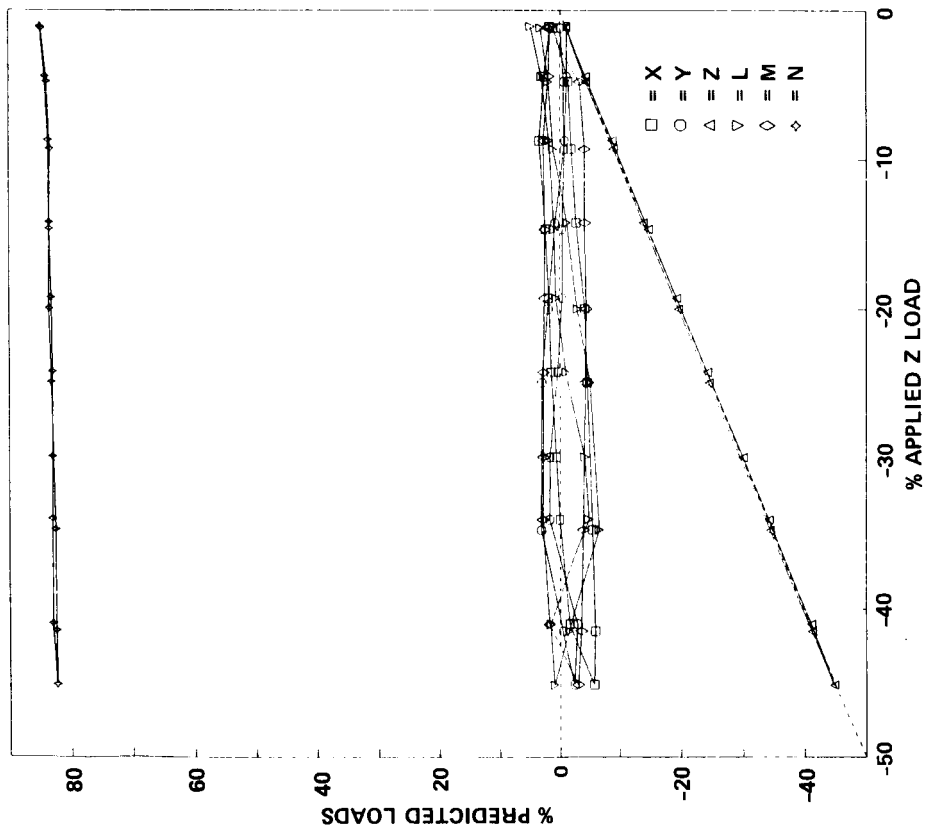


Figure C15.— Responses to applied Z load (heavy-hover triple loads).

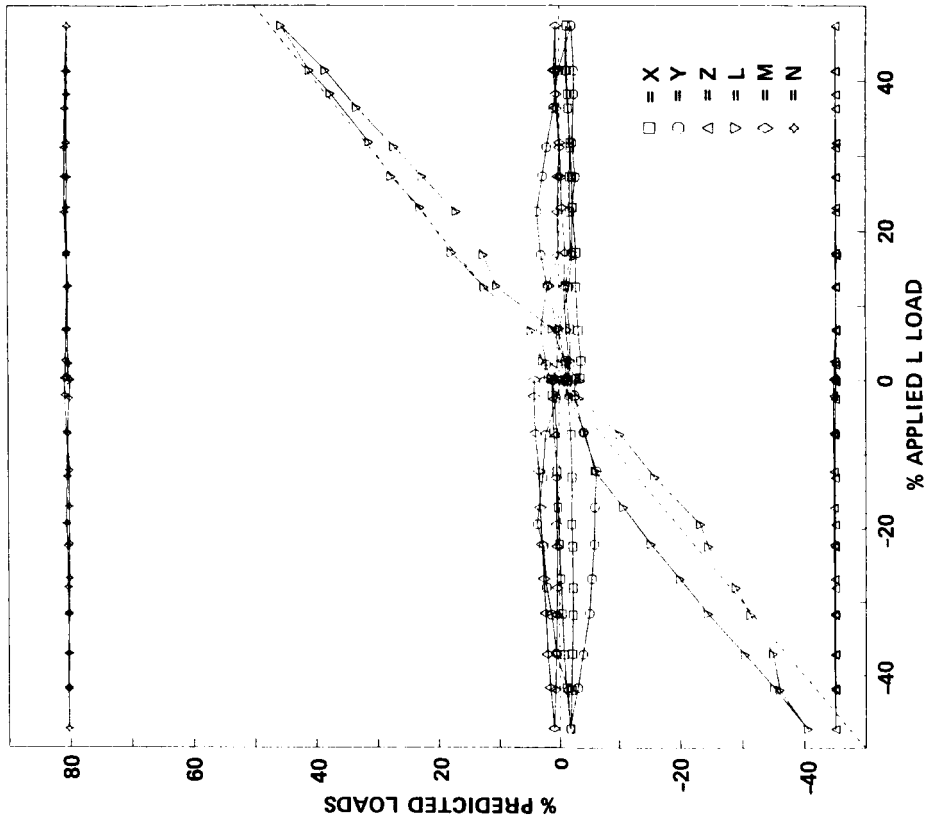


Figure C16.— Responses to applied L load (heavy-hover triple loads).

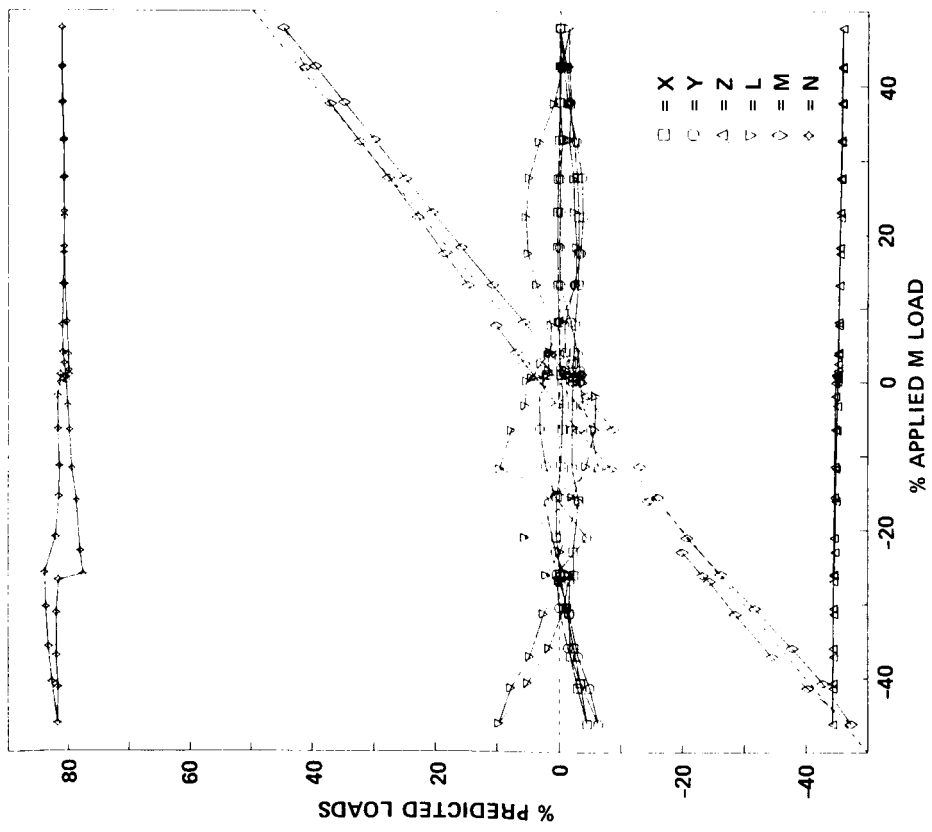


Figure C17.— Responses to applied *M* load (heavy-hover triple loads).

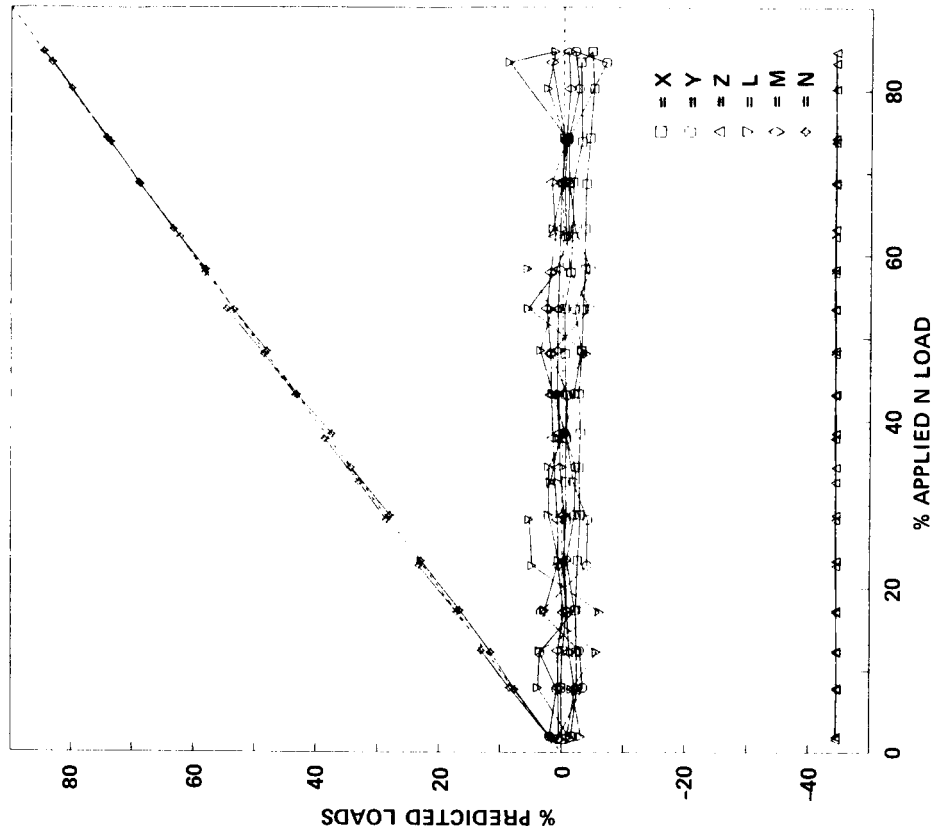


Figure C18.— Responses to applied *N* load (heavy-hover triple loads).

REFERENCES

1. Burks, J. S.: Rotor Systems Research Aircraft (RSRA) Rotor Force and Moment Measurement System. AIAA Paper 81-2516, AIAA/SETP/SFTE/SAE/ITEA/IEEE 1st Flight Testing Conference, Las Vegas, Nevada, Nov. 1981.
2. Acree, C. W., Jr.: Results of the First Complete Static Calibration of the RSRA Rotor-Load-Measurement System. NASA TP-2327, Aug. 1984.
3. Acree, C. W., Jr.: Preliminary Results of the First Static Calibration of the RSRA Helicopter Active-Isolator Rotor Balance System. NASA TM-84395, Nov. 1983.
4. Acree, C. W., Jr.: Numerical Analysis of the First Static Calibration of the RSRA Helicopter Active-Isolator Rotor Balance System. NASA TM-85975, Feb. 1985.
5. Acree, C. W., Jr.: Verification of Static Rotor-Load Measurement Capabilities of the RSRA Helicopter Active-Isolator System. AHS National Specialists' Meeting on Helicopter Testing Technology, Oct. 29-Nov. 1, 1984, Williamsburg, Virginia.
6. Walton, W. C., Jr.; Hedgepeth, R. E.; and Bartlett, F. D., Jr.: Report on Rotor Systems Research Aircraft Design for Vibrations. Paper 760895, SAE 1976 Aerospace Engineering and Manufacturing Meeting, San Diego, California, Nov. 30-Dec. 2, 1976.
7. Kuczynski, W. A.; and Madden, J.: The RSRA Active Isolation/Rotor Balance System-Rotor Systems Research Aircraft. Paper 18, 4th European Rotorcraft and Powered Lift Aircraft Forum, Stresa, Italy, Sept. 13-15, 1978.
8. Jeffery, P.; and Huber, R.: Design and Development of a Motion Compensator for the RSRA Main Rotor Control. Presented at the 13th Aerospace Mechanisms Symposium, NASA Johnson Space Center, Houston, Texas, Apr. 26-27, 1979. NASA CP-2081, pp. 15-25.
9. Acree, C. W. et al.: RSRA Calibration Facility Operations Manual. NASA TM-84389, Aug. 1983.
10. Draper, N. R.; and Smith, H. B.: Applied Regression Analysis. Wiley, New York, 1966.

1. Report No. NASA TM-88211	2. Government Accession No.	3. Recipient's Catalog No.	
4. Title and Subtitle FINAL REPORT ON THE STATIC CALIBRATION OF THE RSRA ACTIVE-ISOLATOR ROTOR BALANCE SYSTEM		5. Report Date March 1987	
		6. Performing Organization Code	
7. Author(s) C. W. Acree, Jr.		8. Performing Organization Report No. A-86115	
		10. Work Unit No.	
9. Performing Organization Name and Address Ames Research Center Moffett Field, CA 94035		11. Contract or Grant No.	
		13. Type of Report and Period Covered Technical Memorandum	
12. Sponsoring Agency Name and Address National Aeronautics and Space Administration Washington, DC 20546		14. Sponsoring Agency Code 505-61-51	
		15. Supplementary Notes Point of contact: C. W. Acree, Jr., Ames Research Center, M/S 237-5, Moffett Field, CA 94035 (415) 694-5423 or FTS 464-5423	
16. Abstract The Rotor Systems Research Aircraft (RSRA) active-isolator system is designed to reduce rotor vibrations transmitted to the airframe and to simultaneously measure all six forces and moments generated by the rotor. These loads are measured by using a combination of load cells, strain gages, and hydropneumatic active isolators with built-in pressure gages. The first static calibration of the complete active-isolator rotor balance system was performed in 1983 to verify its load-measurement capabilities. Analysis of the data included the use of multiple linear regressions to determine calibration matrices for different data sets and a hysteresis-removal algorithm to estimate in-flight measurement errors. Results showed that the active-isolator system can fulfill most performance predictions. The results also suggested several possible improvements to the system.			
17. Key Words (Suggested by Author(s)) Rotor load measurement Helicopter static calibration Rotor systems research		18. Distribution Statement Unclassified - Unlimited Subject Category - 05	
19. Security Classif. (of this report) Unclassified	20. Security Classif. (of this page) Unclassified	21. No. of Pages 40	22. Price* A03

*For sale by the National Technical Information Service, Springfield, Virginia 22161

NASA-Langley, 1987